

**NEUTRON STAR POPULATION DYNAMICS.I:
MILLISECOND PULSARS**

J. M. Cordes

Astronomy Department and NAIC, Cornell University

David F. Chernoff

Astronomy Department, Cornell University

In press *ApJ*, 482, 1997 June 20

ABSTRACT

We study the field millisecond pulsar population to infer its intrinsic distribution in spin period and luminosity and to determine its spatial distribution within the Galaxy. Our likelihood analysis on data from extant surveys (22 pulsars with periods < 20 ms) accounts for the following important selection effects: (1) the survey sensitivity as a function of direction, spin period, and sky coverage; (2) interstellar scintillation, which modulates the pulsed flux and causes a net increase in search volume $\sim 30\%$; and (3) errors in the pulsar distance scale.

Adopting power-law models (with cutoffs) for the intrinsic distributions, the analysis yields a minimum period cutoff $P_{\min} > 0.65$ ms (99% confidence), a period distribution $\propto P^{-2.0 \pm 0.33}$ and a pseudo-luminosity distribution $\propto L_p^{-2.0 \pm 0.2}$ (where $L_p = \text{flux density} \times \text{distance}^2$, for $L_p \geq 1.1$ mJy kpc 2).

We find that the column density of millisecond pulsars (uncorrected for beaming effects) is $\sim 50^{+30}_{-20}$ kpc $^{-2}$ in the vicinity of the solar system. For a Gaussian model the z scale height is $0.65^{+0.16}_{-0.12}$ kpc, corresponding to local number density 29^{+17}_{-11} kpc $^{-3}$. (For an exponential model the scale height becomes $0.50^{+0.19}_{-0.13}$ kpc and the number density 44^{+25}_{-16} kpc $^{-3}$.) Estimates of the total number of MSPs in the disk of the Galaxy and for the associated birthrate are given. The contribution of a diffuse halo-like component (tracing the Galactic spheroid, the halo or the globular cluster density profile) to the local number density of MSPs is limited to $\lesssim 1\%$ of the midplane value.

We consider a kinematic model for the MSP spatial distribution in which objects in the disk are kicked once at birth and then orbit in a smooth Galactic potential, becoming dynamically well-mixed. The analysis yields a column density 49^{+27}_{-17} kpc $^{-2}$ (comparable to the above), a birth z kick velocity 52^{+17}_{-11} km s $^{-1}$ and a 3D velocity dispersion of ~ 84 km s $^{-1}$. MSP velocities are smaller than those of young, long-period pulsars by about a factor of 5. The kinematic properties of the MSP population are discussed, including expected transverse motions, the occurrence of asymmetric drift, the shape of the velocity ellipsoid and the z scale height at birth. If MSPs are long-lived then a significant contribution to observed MSP z velocities owes to diffusive processes that increase the scale height of old stellar populations; our best estimate of

the 1D velocity kick that is unique to MSP evolution is $\sim 40 \text{ km s}^{-1}$ if such diffusion is taken into account.

The scale heights of millisecond pulsars and low-mass X-ray binaries are consistent, suggesting a common origin and that the primary channel for forming both classes of objects imparts only low velocities. Binaries involving a common envelope phase and a neutron-star forming supernova explosion can yield such objects, even with explosion asymmetries like those needed to provide the velocity distribution of isolated, nonspunup radio pulsars.

Future searches for MSPs may be optimized using the model results. As an example, we give the expected number of detectable MSPs per beam area and the volumes of the Galaxy sampled per beam area for a hypothetical Green Bank Telescope all sky survey. Estimates for the volume that must be surveyed to find a pulsar faster than 1.5 ms are given. We also briefly discuss how selection effects associated with fast binaries influence our results.

Subject headings: pulsars, stars-binary:

1. INTRODUCTION

Millisecond pulsars (MSPs) differ from slower-spin pulsars in important ways. First, their spindown rates and derived surface magnetic fields are several orders of magnitude smaller. MSPs have implied fields of $10^{7.9} - 10^9$ Gauss, while pulsars with periods of order one second are characterized by magnetic fields of $10^{11} - 10^{13}$ Gauss. Closely related is the observation that the characteristic spin-down times of MSPs, ranging from several tenths to tens of Gyr, far exceed those of slower-spin pulsars. Some MSPs were born with periods near their present-day values and are, consequently, much younger than their spindown times (Camilo, Thorsett & Kulkarni 1994). However, MSPs are thought to be active as radio pulsars for hundreds to thousands of times longer than strong-field pulsars. Taking active lifetimes into account, it appears that there may be comparable numbers of young pulsars and MSPs in the Galaxy though the birth rate of MSPs is $\sim 10^4$ times smaller.

A second significant difference is that more than 2/3 of MSPs are in binary systems, while young, strong-field pulsars are largely solitary objects, a fact which has both theoretical and observational implications. Clearly, the evolutionary pathways that gives rise to MSPs are integrally related to the interaction of the binary stars (Alpar *et al.* 1982, Ruderman & Shaham 1983; for a general review see Bhattacharya & van den Heuvel 1991). Moreover, searches for MSPs must confront the additional selection effects that mitigate against the detection of accelerated pulsars. As is shown below, detection of the fastest spinning pulsars is inhibited by any effects that smear out the pulse, such as dispersive propagation in the interstellar medium. Orbital motion, uncompensated for in the surveys we analyze here, also smears out pulses according to the change

in velocity over the duration of the observation and is therefore most important for short period pulsars in compact binaries (e.g. Johnston & Kulkarni 1991).

In this paper, we analyze the spatial distribution of MSPs. Our purpose is to derive the best estimates for MSP population parameters through careful consideration of survey sensitivities as a function of pulse period, dispersion measure and other relevant factors. Our census essentially measures the local number density of MSPs, the fall off in number density above the Galactic plane and establishes upper limits on a diffuse, halo-like component of the MSP population. We analyze the implications of the spatial distribution for the kinematics of the MSP population, inferring the diffusive and impulsive velocity increments suffered. We compare predictions of the distribution of proper motions to extant observations, compare the spatial distribution of LMXBs and MSPs, and describe the importance of our determination of the MSP kick velocity for binary evolutionary scenarios. We provide detailed analysis of the influence of selection effects on the discovery of short period pulsars and pulsars in binaries.

Our results have immediate relevance in a number of respects. Recent MSP surveys have been conducted on the premise that the MSPs are essentially isotropically distributed around the Sun, at least to the depths that surveys probe. Our results establish the scale height and show that Arecibo type surveys see beyond it.

The third way that MSPs differ from slow-spin pulsars is in their peculiar space motions. This is one of the main conclusions of the present paper. Kinematic evidence (e.g. Dewey, Cordes & Wolszczan 1988; Cordes *et al.* 1990; Wolszczan 1994; Nice & Taylor 1995; Nicastro & Johnston 1995) suggests that MSPs are low velocity objects, with typical transverse speeds $\lesssim 100 - 200 \text{ km s}^{-1}$. Such velocities are much less than young pulsars, which have an average speed $\sim 500 \text{ km s}^{-1}$ (Lyne & Lorimer 1994; Cordes & Chernoff 1996). Our results allow us to put more stringent, albeit statistical, limits on the MSP velocities than has hitherto been achieved.

The use of the spatial distribution of MSPs as an indirect means for determining their peculiar velocities is more robust than an analysis of proper motion data. The primary reason is that the orbits of MSPs are perturbed significantly from circular motion around the galactic center so that, given their ages ($> 0.1 \text{ Gyr}$), corrections for differential galactic rotation cannot be made. Arnaud & Rothenflug (1981) applied a similar spatial analysis to young, high-field pulsars as a means for determining their velocities. (The methodology is correct but their assumption that high-field pulsars form a steady, relaxed population is not. Today we know that $\sim 25\text{-}30\%$ escape the Galaxy and that many radio pulsars shut off before traveling to the limiting distance for detection.)

Our approach differs in several ways from those taken by other authors. First, we use a likelihood analysis to provide the best estimates of the MSP population parameters, to account accurately for survey selection effects and distance errors, and to express clearly our physical assumptions. Second, we restrict our analysis to pulsars with spin periods $< 20 \text{ ms}$. We do so because it appears that these neutron stars (NS) are distinct from other pulsars that may have undergone accretion-driven spinup but were left with longer periods (Bhattacharya & van

den Heuvel 1991). We also consider them to be distinct from the higher mass NS-NS binaries, which have pulsars with longer pulse periods (B1913+16, $P = 59$ ms [Taylor & Weisberg 1989]; B1534+12, $P = 38$ ms [Wolszczan 1991]). Third, our approach includes the effects of interstellar scintillations, which modulate the pulsar flux density and influence the rate of detection in surveys.

The paper is organized as follows. In §2 we discuss sensitivities of pulsar surveys and derive quantities that are needed in our analysis. A preliminary attack on the problem is given in §3 where we present a ‘ V/V_{max} ’ analysis, analogous to that used on quasars and gamma-ray burst sources, in order to illustrate the uncertainties involved in pulsar surveys. We derive the survey likelihood function in §4 and apply it in §5 to a disk-only distribution of MSPs. In §6 we apply the analysis to a disk model based on numerical integration of NS orbits in the galactic potential. We consider a combined disk and diffuse halo-like model in §7. Sections 8-11 present the implications of our results for the MSP birthrate, the origins of MSPs and their velocities, and for the optimization of MSP surveys. In §14 we summarize the paper.

2. PULSAR SURVEYS

2.1. Minimum Detectable Flux S_{min}

A pulsar survey has a minimum detectable flux density S_{min} that depends on radiometer noise, the pulse shape, and details of the Fourier analysis used to find pulsars. In Appendix A we derive S_{min} for surveys, which includes pulse broadening effects (from interstellar dispersion and scattering and from detector time constants) and the effects of flux variations from interstellar scintillations (Appendix B), which are strong for the MSP surveys.

For a given direction, the minimum detectable flux density is a function of pulse width and period and radiometer-noise level. The minimum detectable flux density is a function of direction (galactic coordinates ℓ, b), dispersion measure [$DM = \int_0^D dx n_e(x)$, where n_e is the free-electron density and D is the pulsar distance], radio frequency (ν), bandwidth ($\Delta\nu$) and the number of channels (N_{ch}), as well as system temperature (T_{sys}), telescope gain (G), the intrinsic pulse duty cycle, and additional survey dependent factors:

$$S_{min} = S_{min}(\ell, b, P, DM, \nu, \Delta\nu, N_{ch}, T_{sys}, G, \dots). \quad (1)$$

S_{min} depends on additional, unspecified parameters, especially those that describe orbital motion. In most of this paper we ignore such motion; however in §11 we discuss survey biases against short period binaries and their possible effects on our conclusions. In Figure 1 we show S_{min} plotted against period for several values of DM. These curves apply for drift-scan surveys made with the Arecibo telescope at 0.43 GHz toward the galactic pole and at zero zenith angle. We have used a numerical version of a 408 MHz survey (Haslam *et al.* 1982) to calculate the background sky temperature. We assume a Gaussian pulse shape with 3% intrinsic duty cycle. While this duty cycle is shorter than those of some MSPs, the duty cycle and, hence, S_{min} , is dominated

by extrinsic pulse broadening from dispersion, scattering and instrumentation. Pulse broadening from scattering is taken into account by estimating it from large scale galactic models for the electron density, as described by Cordes *et al.* (1991) and Taylor & Cordes (1993; hereafter TC).

The maximum distance to which a particular pulsar is detectable, D_{max} , is given by

$$D_{max} = \left[\frac{L_p}{S_{min}} \right]^{1/2}. \quad (2)$$

We use the ‘pseudo-luminosity’, $L_p \equiv SD^2$, that is often adopted in population studies of pulsars. Though it is preferable to use a physical luminosity (i.e. expressed in units of erg s^{-1}) in analyzing pulsar statistics (Chernoff & Cordes 1996a), estimation of physical luminosities for MSPs is not yet possible because we do not understand radio beaming in MSPs to the same extent that we do for young, strong-field objects (Backer 1976; Rankin 1983; Lyne & Manchester 1988; Rankin 1993). Note that S_{min} depends implicitly on the dispersion measure in a given direction which, in turn, depends on D_{max} . For this reason, D_{max} must be found iteratively.

Figure 2 shows (as solid lines) S_{min} plotted against distance for several values of pulse period and for several directions. These curves illustrate the strong dependence of S_{min} on direction and period. The dashed line indicates the inverse square-law variation of flux density for a source of 30 mJy at a distance of 1 kpc. The intersection points of the dashed and solid curves determine the maximum distances D_{max} that a pulsar can be seen for the different cases.

From D_{max} , the total volume to which the survey is sensitive in a given beam area is

$$V_{max} = \frac{1}{3} \Omega_b D_{max}^3. \quad (3)$$

Because of the strong period and luminosity dependence of D_{max} and, hence, V_{max} , the latter quantity may be used to determine the period and luminosity distributions of MSPs.

2.2. MSP Surveys: Properties, Volumes and Distances Sampled

We have applied the likelihood analysis to 8 pulsar surveys that have been reported in the literature. Six use the Arecibo telescope, yielding 11 MSPs, the seventh is the Parkes southern-hemisphere survey that yielded 10 MSPs, as reported by Manchester (1994) when the survey was about 75% complete.¹ The eighth survey is the Jodrell Bank survey, a portion of which has been reported in the discovery of the MSP J1012+5307 (Nicastro *et al.* 1995). We have not included J0218+4232 (Navarro *et al.* 1995) because it was discovered in an aperture synthesis survey with selection criteria quite different from the periodicity searches of the surveys

¹The final tally of the Parkes survey is 17 MSPs with all data analyzed, of which $\sim 95\%$ was relatively free of RFI (M. Bailes, private communication).

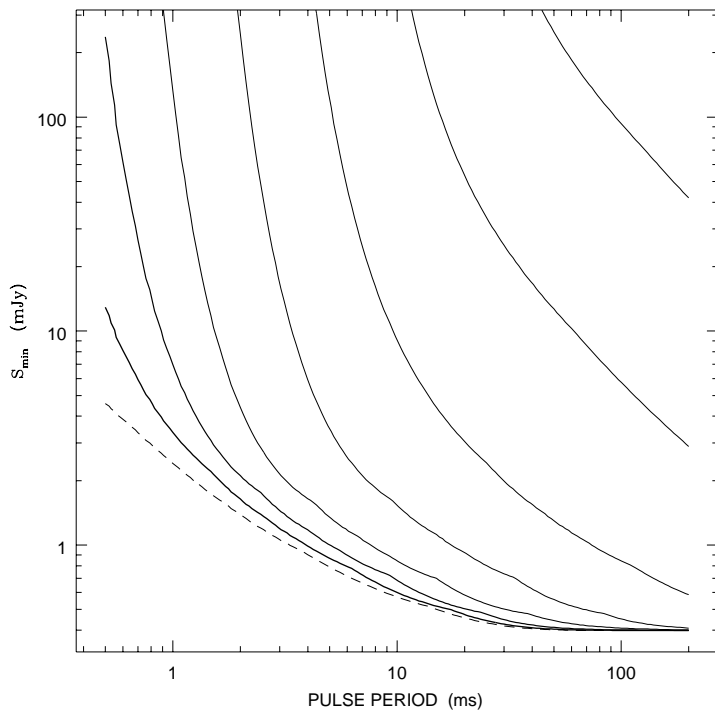


Fig. 1.— Plot of minimum detectable flux density vs. pulse period for a typical survey at Arecibo. The different curves are for dispersion measures $DM = 0$ (dashed line) and $DM = 10 \times 2^n$, with $n = 0, 1, \dots$ (solid lines, left to right) and apply to observations toward the galactic poles and at zero zenith angle.

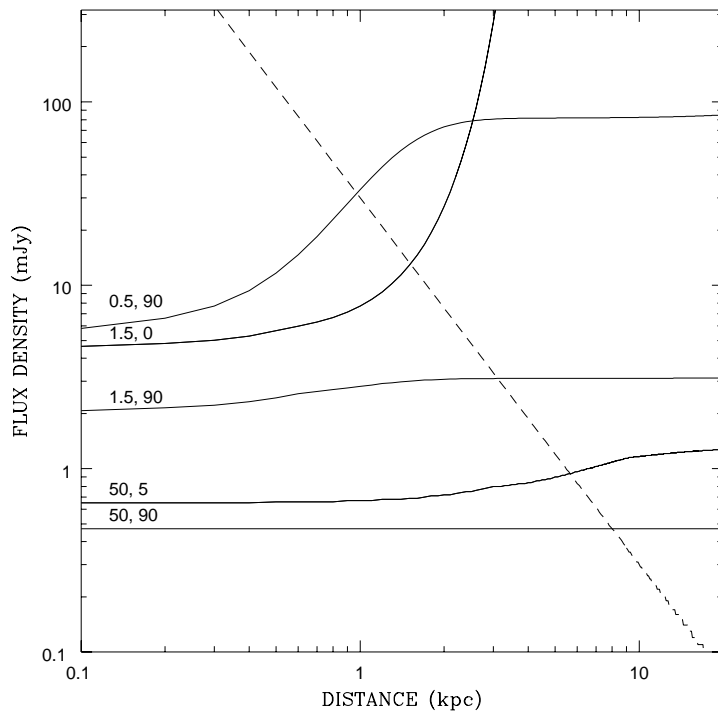


Fig. 2.— (Solid lines:) Minimum detectable flux density for an Arecibo survey for the labelled pulse periods (ms) and galactic latitudes (deg). The plotted values apply for sources viewed at the telescope beam center. At the beam half-power point, the values are doubled. (Dashed line:) The inverse-square law variation of flux density for a source with 30 mJy when at a 1-kpc distance. The distances where the solid lines cross the dashed line are values of D_{max} , the maximum distance at which the particular object could be detected. At the beam half-power point, the maximum distances are smaller.

we consider. In a future analysis of the distributions of MSP orbital parameters, we will extend our analysis to synthesis surveys.

Table 1 lists the surveys we have used. The columns include the (1) survey number (an arbitrary choice based solely on the order in which we analyzed the surveys); (2) observatory site for the survey; (3) survey frequency; (4) solid angle of interference-free observations; (5) number of MSPs found in the survey; (6) system temperature of the telescope, expressed in Janskys, for observations at the zenith and toward the Galactic poles; (7) minimum flux density for detection of long-period pulsars at the zenith and toward the Galactic poles; and (8) survey reference number.

Table 2 lists the MSPs used in our analysis. Figure 3 shows the total volume searched in each of the 8 programs as a function of spin period for a fixed luminosity of 16 mJy kpc². The Parkes survey by itself has searched the largest volume. The Arecibo surveys in aggregate cover a comparable volume, a few kpc³ for a period of 5 ms. For comparison, the lower panel in Figure 3, shows the maximum distance surveyed, $\langle D_{max} \rangle$, averaged over all directions searched in a given survey. The Arecibo surveys probe about 3 times more deeply than the Parkes survey.

As we demonstrate in this paper, deep, high-latitude surveys at Arecibo (see references below) sample distances that are well beyond the scale height of the population, while the southern-hemisphere Parkes survey, covering a larger area on the sky but being less sensitive at most periods, is better optimized to finding MSPs. We note that the Arecibo search volumes that are devoid of MSPs provide the most stringent constraints on the scale height of MSPs, whereas the totality of detected MSPs essentially determines the local MSP number density.

3. V/V_{max} FOR MILLISECOND PULSARS

The main method of analysis in this paper uses a likelihood function to determine intrinsic properties of the MSP population after accounting for survey selection effects embodied in S_{min} , as calculated above. Here, we motivate our discussion by applying a V/V_{max} analysis to MSP surveys. Consider the line of sight to a MSP discovered in a survey. Subsequent observations yield precise determinations of P, DM, ℓ , b. The flux density is S_d at the time of discovery and S as a long time average. The flux density is time dependent, owing predominantly to refractive and diffractive interstellar scintillation (DISS; e.g. Rickett 1990; Kaspi & Stinebring 1992, Stinebring & Condon 1990; Cordes, Weisberg & Boriakoff 1985). A distance estimate derives from DM and the TC model for the interstellar electron density. The model and, in some cases, auxiliary measurements (timing parallax, neutral-hydrogen absorption, and association with supernova remnants; Frail & Weisberg 1990) yield a range of possible distances, $[D_L, D_U]$.

The volume between us and a given pulsar in a beam of solid angle Ω_b is

$$V = \frac{1}{3} \Omega_b D^3. \quad (4)$$

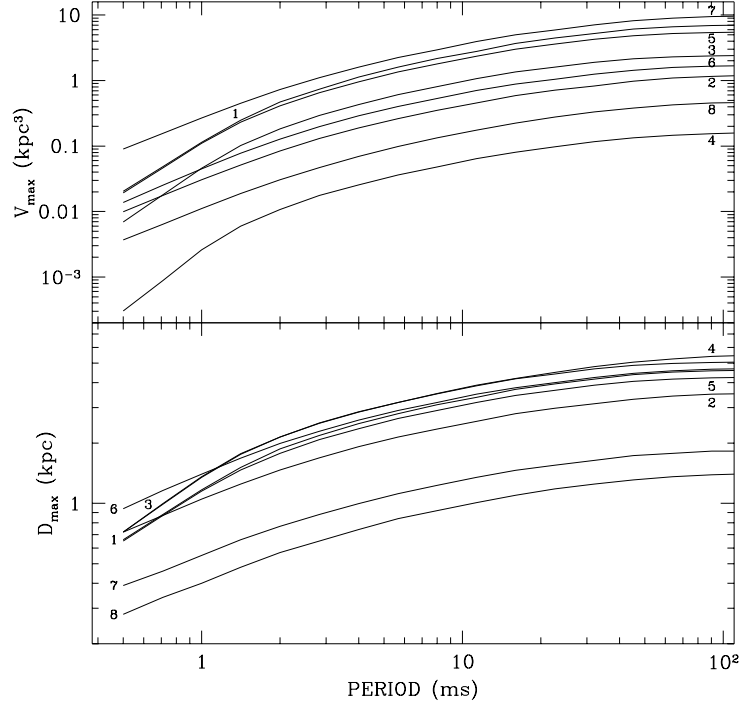


Fig. 3.— (Top:) Volume searched as a function of spin period for a pseudo luminosity $L_p = 16$ mJy kpc 2 labelled by survey number as given in Table 1. (Bottom:) Maximum survey distance, D_{max} , averaged over direction for each of the eight surveys and for a luminosity of 16 mJy kpc $^{-2}$.

The ratio of V to V_{max} from Eq. 3, may then be written as

$$\frac{V}{V_{max}} = \left(\frac{S_{min}}{S} \right)^{3/2}. \quad (5)$$

Applicaton of Eq. 5 involves subtleties that depend on whether the flux density reported for a given object is influenced by the random process associated with DISS. DISS generally *increases* the volume in which a pulsar can be detected (cf. Appendix B). Saturated DISS that is not quenched by time-bandwidth averaging modulates the flux density by a random variable drawn from an exponential probability density function (pdf). Though the modulation is less than unity more often than not, the net effect is to increase the volume by a factor $\Gamma(5/2) \sim 1.33$.

Figure 4 shows V/V_{max} for field MSPs plotted against $|z| = D \sin |b|$. Horizontal error bars reflect uncertainties in the measured flux density and distance errors, the latter also determining the vertical error bars on $|z|$. In most cases, we have used the 400 MHz flux density reported by Taylor, Manchester & Lyne (1993), which is usually an average of many observations and is influenced minimally by DISS. Flux calibrations are typically only about 20% accurate. Weak pulsars can appear brighter than average due to DISS at the time of discovery, however, so the discovery flux $S_d > S_{min}$ while $S < S_{min}$. For these cases (J0034-0534 and J0711-6830), $V/V_{max} \rightarrow 1$. The intrinsically brightest MSP, B1937+21, is detectable to only ~ 8 kpc despite its large luminosity $L_p \gtrsim 3100$ mJy kpc² because, at its low galactic latitude, dispersion and scattering effects grow rapidly with distance. Consequently, we argue that the claimed upper distance limit, $D_U \sim 15.7$ kpc, is a factor of two too large. The moderate-latitude pulsar J1643-1224 is attributed only a lower bound on its distance by the TC model, $D > 4.8$ kpc, because its DM cannot be accounted for by the model. We suspect that this pulsar's DM is enhanced by unmodeled ionized gas along the line of sight and that the distance is most likely less than 4.8 kpc. In the absence of further data, however, we use the distance lower bound as is.

Apart from the pulsar with a questionable distance estimate (J1643-1224), Figure 4 shows that MSPs are to be found at only low values of $|z|$, suggesting, therefore, that the scale height for MSPs is $\sim 0.5\text{-}1$ kpc. To properly estimate the scale height requires careful accounting of selection effects in MSP surveys, as we do in §4. However, Arecibo surveys at high latitudes search to several kpc for typical luminosities. The absence of high $|z|$ pulsars is therefore especially striking. The Arecibo MSPs also tend to have small values of V/V_{max} , as would be expected for surveys that search well beyond the scale height of the population.

4. LIKELIHOOD ANALYSIS

4.1. Observables, Assumptions and Statistical Method

A survey for MSPs typically searches many beam areas for each MSP discovery. The spatial distribution of MSPs determines this yield, along with the survey sensitivity as a function of

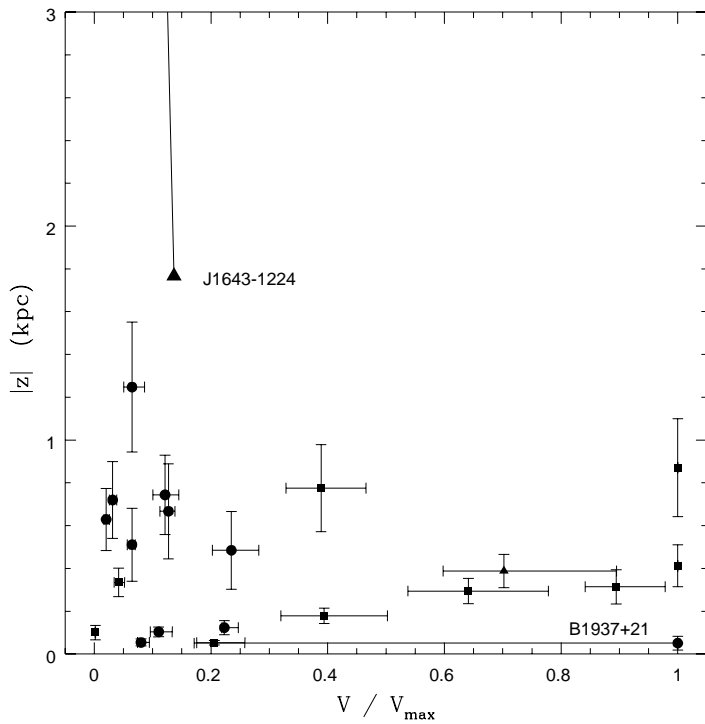


Fig. 4.— A plot of $|z|$ vs. V/V_{\max} for field millisecond pulsars. Filled circles denote pulsars discovered at Arecibo. Filled squares indicate MSPs found at Parkes and Jodrell Bank. The filled triangle denotes the lower bound on z and V/V_{\max} for J1643-1224, whose distance estimate is only a lower bound, as discussed in the text.

period, the period distribution, and the luminosity function. Here we derive the likelihood function for a survey, taking these factors into account. We take as observables the directions of all beam areas searched, the survey sensitivities in these directions, and the parameters that describe individual pulsars, including direction, period, flux density, and dispersion measure. We also use distance estimates based primarily on the electron density model of TC. Such distances are imprecise and our method takes into account the large uncertainties in distance that translate into large uncertainties in implied luminosity.

Consider a telescope beam with solid angle Ω_b . The mean number of MSPs expected in the beam per unit period, luminosity and distance is

$$\frac{\partial^3 \langle N_p \rangle}{\partial P \partial L_p \partial D} = \Omega_b D^2 n_p(D, \ell, b) f_{L_p}(L_p) f_P(P), \quad (6)$$

where the number density of MSPs, $n_p(D, \ell, b)$, is an arbitrary function of position. We have assumed that the joint probability distribution of period P , luminosity L_p and position is *factorable*. The physical assumption is that the distribution in space is independent of the distribution of intrinsic pulsar properties (P and L_p) and, furthermore, that P and L_p are uncorrelated. We write the period pdf, $f_P(P)$, and luminosity pdf, $f_{L_p}(L_p)$, each with unit normalization. With the small number of MSPs currently available there is scant evidence that the factorization is or is not appropriate; however, in the future, our method can be applied easily to more complicated joint distributions if warranted. In particular, we defer to another paper exploration of the joint statistics of L_p and P . Below, we specialize to disk and disk + diffuse models and we take into account the variation of the telescope gain across the its beam.

To calculate the mean number of MSPs expected per beam, we integrate Eq. 6 to obtain

$$\langle N_p \rangle = \Omega_b \int dP f_P(P) \int dL_p f_{L_p}(L_p) \int_0^{D_{max}} dDD^2 n_p(D, \ell, b). \quad (7)$$

The volume searched per beam, averaged over P and L_p , is

$$\delta V_s = \frac{\Omega_b}{3} \int dP f_P(P) \int dL_p f_{L_p}(L_p) D_{max}^3. \quad (8)$$

Survey sensitivities are implicit in D_{max} , as discussed in §2. For detections, we take into account the constraints that exist, due to post-discovery observations, on period, flux density, and distance: $P \pm \Delta P/2$, $S \pm \Delta S/2$, and $D \in [D_L, D_U]$. Integrating over the subvolume bounded by these constraints, the mean number of MSPs is

$$\begin{aligned} \langle N_p \rangle_D &= \Omega_b \int_{P \pm \Delta P/2} dP f_P(P) \int_{D_L}^{\min[D_U, D_{max}]} dDD^4 n_p(D, \ell, b) \int_{S \pm \Delta S/2} dS' f_{L_p}(S'D^2) \\ &= \Omega_b \int_{P \pm \Delta P/2} dP f_P(P) \int_{S_1 D_L^2}^{S_2 D_U^2} dL_p f_{L_p}(L_p) \int_{\max[D_L, (L_p/S_2)^{1/2}]}^{\min[D_U, D_{max}, (L_p/S_1)^{1/2}]} dDD^2 n_p(D, \ell, b), \end{aligned} \quad (9)$$

where $S_{1,2} \equiv S \mp \Delta S/2$. For each known pulsar, D_{max} is the maximum distance for the survey that could have detected each pulsar. Several MSPs in our analysis were first discovered in other surveys but were subsequently detected (rediscovered) in one of the eight surveys and we analyze them accordingly. For a given beam, the Poisson probabilities for detecting zero or one MSP are

$$\begin{aligned} P_0 &= e^{-\langle N_p \rangle} \\ P_1 &= \langle N_p \rangle e^{-\langle N_p \rangle}. \end{aligned} \quad (10)$$

We construct the survey likelihood function as the product of nondetection (ND) and detection (D) factors:

$$\mathcal{L} = \mathcal{L}_{ND} \mathcal{L}_D, \quad (11)$$

where, for N_b total beams searched, M_p MSPs found, and assuming $\langle N_p \rangle \ll 1$,

$$\mathcal{L}_{ND} = \exp \left(- \sum_{j=1}^{N_b} \langle N_p \rangle_j \right) \quad (12)$$

$$\mathcal{L}_D = \prod_{k=1}^{M_p} \langle N_p \rangle_{D_k}. \quad (13)$$

The log likelihood is

$$\Lambda \equiv \ell n \mathcal{L} = - \sum_{j=1}^{N_b} \langle N_p \rangle_j + \sum_{k=1}^{M_p} \ell n \langle N_p \rangle_{D_k}. \quad (14)$$

The likelihood function may be simplified if we factor the pulsar number density into a constant n_0 times a shape factor:

$$n_p(D, \ell, b) = n_0 h(D, \ell, b), \quad (15)$$

where $h(D, \ell, b)$ is dimensionless and has a maximum of unity. Substituting, the likelihood function becomes

$$\Lambda(\boldsymbol{\theta}, n_0) = M_p \ell n n_0 - n_0 V_d + \sum_{k=1}^{M_p} \ell n \delta V_p, \quad (16)$$

where the vector $\boldsymbol{\theta}$ denotes the set of parameters other than n_0 . We define the *survey detection volume* as the sum over beams,

$$V_d = \sum_{j=1}^{N_b} \delta V_{dj}, \quad (17)$$

where (dropping beam labels)

$$\delta V_d = \frac{\partial \langle N_p \rangle}{\partial n_0}. \quad (18)$$

and the constrained subvolume per discovered MSP is

$$\delta V_p = \frac{\partial \langle N_p \rangle_D}{\partial n_0}. \quad (19)$$

The survey detection volume V_d is the volume searched weighted by the dimensionless MSP space density, h . The expected number of MSPs in a survey is simply $n_0 V_d$. Eq. 16 applies to a single-component density model, such as the disk distribution we consider in the next two sections. Multiple components require the alternative treatment of §7.

Maximizing \mathcal{L} with respect to n_0 , we obtain the best fit number density (for a specific set of parameters, $\boldsymbol{\theta}$)

$$\hat{n}_0 = \frac{M_p}{V_d}. \quad (20)$$

Substituting, the log likelihood becomes

$$\Lambda(\boldsymbol{\theta}, \hat{n}_0) = M_p \ln \hat{n}_0 - M_p + \sum_{k=1}^{M_p} \ln \delta V_p. \quad (21)$$

For $n_0 \neq \hat{n}_0$, the variation in the log likelihood is

$$\Lambda(\boldsymbol{\theta}, n_0) - \Lambda(\boldsymbol{\theta}, \hat{n}_0) = M_p \left[\ln \left(\frac{n_0}{\hat{n}_0} \right) - \left(\frac{n_0 - \hat{n}_0}{\hat{n}_0} \right) \right] \approx -\frac{M_p}{2} \left(\frac{n_0 - \hat{n}_0}{\hat{n}_0} \right)^2, \quad (22)$$

where the approximate, quadratic form holds for $|n_0 - \hat{n}_0|/\hat{n}_0 \ll 1$.

We want to know the marginal distribution of each parameter. For a given parameter $\theta_j \in \boldsymbol{\theta}$, the marginal pdf is the normalized integral over all other parameters

$$f_{\theta_j}(\theta_j) = \frac{\int_{exc.\theta_j} d\boldsymbol{\theta} \int dn_0 \mathcal{L}(\boldsymbol{\theta}, n_0)}{\int d\boldsymbol{\theta} \int dn_0 \mathcal{L}(\boldsymbol{\theta}, n_0)} \approx \frac{\int_{exc.\theta_j} d\boldsymbol{\theta} \mathcal{L}(\boldsymbol{\theta}, \hat{n}_0) \hat{n}_0}{\int d\boldsymbol{\theta} \mathcal{L}(\boldsymbol{\theta}, \hat{n}_0) \hat{n}_0}, \quad (23)$$

where the integral subscript ‘exc. θ_j ’ means that all parameters except the j^{th} one are integrated over. The approximate form in Eq. 23 assumes a sharp peak about \hat{n}_0 and becomes an increasingly good approximation as M_p grows. The marginal pdf for n_0 is

$$f_{n_0}(n_0) = \frac{\int d\boldsymbol{\theta} \mathcal{L}(\boldsymbol{\theta}, n_0)}{\int d\boldsymbol{\theta} \int dn_0 \mathcal{L}(\boldsymbol{\theta}, n_0)} \approx \left(\frac{M_p}{2\pi} \right)^{1/2} \frac{\int d\boldsymbol{\theta} \mathcal{L}(\boldsymbol{\theta}, \hat{n}_0) e^{-\frac{M_p}{2} \left(\frac{n_0 - \hat{n}_0}{\hat{n}_0} \right)^2}}{\int d\boldsymbol{\theta} \mathcal{L}(\boldsymbol{\theta}, \hat{n}_0) \hat{n}_0}. \quad (24)$$

For disk models the areal, or column, density of MSPs is less model dependent than the number density and scale height separately. The column density is $N_0 \equiv \eta n_0 \sigma_z$, where η is a dimensionless factor of order unity and σ_z is a scale-height parameter. The pdf of N_0 is calculated by marginalizing \mathcal{L} over all parameters except n_0 and σ_z . The resultant joint pdf f_{n_0, σ_z} is then integrated according to:

$$f_{N_0}(N_0) = \eta^{-1} \int d\sigma_z \sigma_z^{-1} f_{n_0, \sigma_z}(N_0/\eta\sigma_z, \sigma_z). \quad (25)$$

For disk models considered below, $\eta = 2$ for an exponential in z and $\eta = \sqrt{2\pi}$ for a Gaussian in z .

4.2. Telescope Gain

MSP surveys usually involve drift scans or sustained pointings toward specific sky positions. The telescope’s gain toward a given source varies over the analyzed portion of the drift scan and is a function of the source’s position relative to the beam center (see, e.g., Camilo, Nice & Taylor 1996). We account for gain variations by replacing the beam solid angle Ω_b in Eq. 7 with a sum over equal solid-angle terms

$$\Omega_b \rightarrow \sum_{m=1}^{n_g} \delta\Omega_b, \quad (26)$$

where the telescope gain varies with m , G_m . The minimum detectable flux density S_{min} is therefore a function of m . For some drift-scan surveys, we take into account that the data are analyzed in data blocks that overlap by some fraction (usually 50%).

For drift scans, G varies with time over the data set and the offset from the beam center in declination is also taken into account. The sum in Eq. 26 becomes a sum over discrete steps in declination. For pointed (tracking) observations, we use actual pointing directions and break the beam into equal-solid angle annuli about the beam center, which we sum over as in Eq. 26. We find that only a small number of subbeam elements is needed to account for the shape of the beam, e.g. $n_g \sim 2$ or 3.

4.3. Interstellar Scintillations

In Appendix B we derive the effects of diffractive interstellar scintillations on flux densities and on the (pseudo) luminosity function. To use these results, we replace f_{L_p} in Eq. 7 with the corresponding ‘scintillated’ luminosity function, f'_{L_p} , as defined in the Appendix. We do so for surveys assuming that specific sky positions are observed only once. However, we use the unscintillated luminosity function in Eq. 10 because flux densities reported for the known pulsars are generally long-term averages of many independent measurements.

4.4. Comparison with Other Statistical Methods

Our statistical method differs substantially from other studies of the MSP population. A common approach to population studies, including pulsars and gamma-ray bursts, makes use of nonparametric estimators. The rationale is to try to draw inferences about certain properties of the population without assuming a specific class of models. In contrast, our likelihood analysis makes very specific assumptions about the class of models to be examined; for example, we have assumed *a priori* that all probability distributions are continuous. The differences between parametric and nonparametric treatments highlights some of the strengths and weaknesses of our approach.

It has been shown (Loredo and Wasserman 1995) that nonparametric estimators may be derived from a special maximum likelihood model solution. Since our parametric treatment is also based on a maximum likelihood analysis, it is straightforward to study the relationship between alternative methodologies by making a comparison of the assumptions made in the two searches. The special solution leading to the nonparameteric estimators of interest comes from a search for a maximum likelihood solution amongst all functions and generalized distributions (i.e. delta functions) with equal *a priori* weight. This class of functions is so large that the most likely model is *always* one which exactly and precisely describes the observed data; thus, nonparametric estimators satisfy the rationale for which they are introduced. This contrasts with the parametric treatment adopted here for which the class of functions is (by comparison) extremely small. We liken nonparameteric estimators to models with large numbers of free parameters.

In deciding what treatment to adopt, it is helpful to appeal to the Bayesian odds ratio to decide whether adding a new parameter to a model is justified by the better description of the data it may entail. Roughly speaking each newly added parameter will improve the quality of the model's description of the data. The odds ratio allows a quantitative decision to be made whether to adopt the more complex model by weighing the improvement in the description against the additional freedom to fit arbitrary data sets. The situation for the MSP's is that the population is rather small and we have anticipated (without any detailed investigation) that the odds ratio will favor models with relatively small numbers of parameters. We have therefore focused in this paper on parameteric methods with small numbers of parameters.

An additional factor in our choice of parametric methods is that it is straightforward to include ancillary information about the population (e.g. continuity of the model), whereas in nonparametric approaches such constraints are difficult to incorporate. Moreover, we find the parametric approach naturally allows the inference of population parameters of significant interest (e.g. cutoffs in the period distribution).

The main drawback of the parametric approach is that the results apply only to the particular set of models that the parameters can describe. If the real data were much better described by some completely different unstudied model, one would have no indication of that fact. In this paper we have considered several plausible models but these cannot begin to describe all possibilities.

A number of pulsar population studies are based in whole or in part on such estimators (Vivekenand & Narayan 1981, hereafter VN; Phinney & Blandford 1981 and Narayan 1987). To be a bit more descriptive, in the VN method a scale factor is calculated for each object detected in a survey. The factor represents how many pulsars with the same period P and luminosity L_p

exist in the Galaxy given the fraction of the Galaxy searched. In our notation, the scale factor is

$$\mathcal{S}(P, L_p) = \frac{\sum_{\text{full sky}} \Omega_{bj} \int_0^{\infty} dD D^2 n_p(D, \ell, b)}{\sum_{j=1}^{N_b} \Omega_{bj} \int_0^{D_{max}} dD D^2 n_p(D, \ell, b)}, \quad (27)$$

where D_{max} , as before, depends on many survey and pulsar parameters, including P and L_p . The number of pulsars in the Galaxy is then calculated through a sum over detected pulsars as

$$N_{gal} \approx \sum_{i=1}^{N_{msp}} \mathcal{S}(P_i, L_{p_i}). \quad (28)$$

The resultant total number of pulsars is a *mean value* similar in nature to the mean value of the number density, \hat{n}_0 , that we have calculated. One drawback is that the VN method estimates the number of pulsars in the Galaxy *exactly* like those actually detected. In other words, it explicitly includes contributions to the mean only at the periods and luminosities of the known pulsars. It is inherently discrete as compared to our likelihood method based on continuous distributions. Another drawback is that the method does not directly allow computation of confidence intervals. Finally, since the scale factors are calculated only for the detected pulsars, there is no means for estimating the cutoffs of the distributions of P and L_p . Below we compare our results on MSPs to those of Lorimer *et al.* (1995) and Bailes & Lorimer (1995; hereafter BL) with these issues in mind.

5. DISK MODEL FOR MILLISECOND PULSARS

5.1. Method

The simplest spatial model is a disk with constant scale height σ_z , so that the density is a function of z only. We let $n_p(z) = n_d h_p(z)$ with $h_p(0) = 1$, where n_d is the midplane density that corresponds to n_0 in §4.

The parameters to be solved for describe the period, luminosity and z distributions, $f_P(P)$, $f_{L_p}(L_p)$ and $n_p(z)$. We have considered three models for $h_p(z)$: (1) a Gaussian function in z with an rms value of z given by σ_z ; (2) an exponential model with 1/e scale height σ_z ; and (3) a numerically derived distribution of NS orbits, neither Gaussian nor exponential in form, discussed in §6. For the luminosity and period pdfs, we adopt power-law functions, i.e. $f_{L_p} \propto L_p^{-\alpha_{L_p}}$ and $f_P \propto P^{-\alpha_P}$, with respective lower and upper cutoffs, L_{p1}, L_{p2} and P_1, P_2 .

The greatest computational effort goes into calculation of \mathcal{L}_{ND} (Eq. 12). We computed it efficiently by summing the D integral in Eq. 7 over the survey beam areas for a grid of σ_z , P , and L_p ; as stated before, we use the scintillation-modified luminosity function in this computation.

Next we form the likelihood for different model parameters $\alpha_{L_p}, \alpha_P, L_{p_1}, L_{p_2}, P_1, P_2$ by calculating integrals over P and L_p with weights f_P and f_{L_p} (cf. Eq. 7).

We maximized Λ by varying the parameters (or subsets of the parameters) over a grid. We kept the upper cutoffs on the period and luminosity distributions fixed at $P_2 = 20$ ms and $L_{p_2} = 16,000$ mJy kpc². The period cutoff corresponds to the selection used to define the sample. Since the number of objects decreases rapidly as P increases, the upper cutoff plays little role in any of the results below. The luminosity cutoff corresponds to the maximum possible luminosity in the observed sample. We also tested the effects of varying L_{p_2} and found that results are not sensitive to this parameter. Exclusion of B1937+21, the most luminous MSP, allows a much smaller value for L_{p_2} to describe the remaining 21 pulsars in the sample; but none of the other results below are substantially altered.

5.2. Results

The five parameters ($P_1, L_{p_1}, \alpha_{L_p}, \alpha_P$, and σ_z) were varied over a grid to find the maximum Λ . We formed marginal pdfs according to Eqs. 23 and 24. Results are summarized in Table 3. Figure 5 shows the marginal pdfs for each of the six parameters (the above-mentioned five and the number density, n_d). Using these pdfs, we calculated the confidence intervals on the parameters that are given in Table 3. The maxima are well-defined and easily located.

5.2.1. Minimum Period P_1 and Period Distribution Slope α_P

Naturally P_1 must be less than or equal to the period of the shortest-period MSP in our sample. When other parameters are held fixed, it is straight forward to show that Λ must decrease as P_1 is made smaller. The best-fit, minimum period lies only slightly below that of the most-rapidly-spinning, known pulsar, B1937+21 (1.56 ms). However, the data allow $P_1 < 1.56$ ms at a reduced level of confidence. The results are given in Table 3 for both the Gaussian and exponential models. The cutoff is > 1 ms at 95% confidence and > 0.65 ms at 99% confidence.

The period distribution falls off steeply with period, implying the existence of many objects at small P ($dN/dP \propto f_P \propto P^{-2.0 \pm 0.33}$). It is well known that physical instabilities will act on neutron stars with very short rotation periods. Ignoring the magnetic field and assuming accretion from an inner edge of a Keplerian disk, Cook *et al.* (1994a,b) have shown that $1.4M_\odot$ neutron stars can be spun up to critical rotation periods (well under 1 ms) for a variety of equations of state without triggering radial instability, e.g. exceeding the maximum neutron star mass. (The results do not assure stability against non-radial modes and the associated gravitational wave emission.) Our overall fit for the period distribution suggests the existence of MSPs faster than those that are currently known (1.56 ms) in view of the fact that the theoretical stability analyses do not rule out such objects. Of course, there may be evolutionary reasons that such objects do

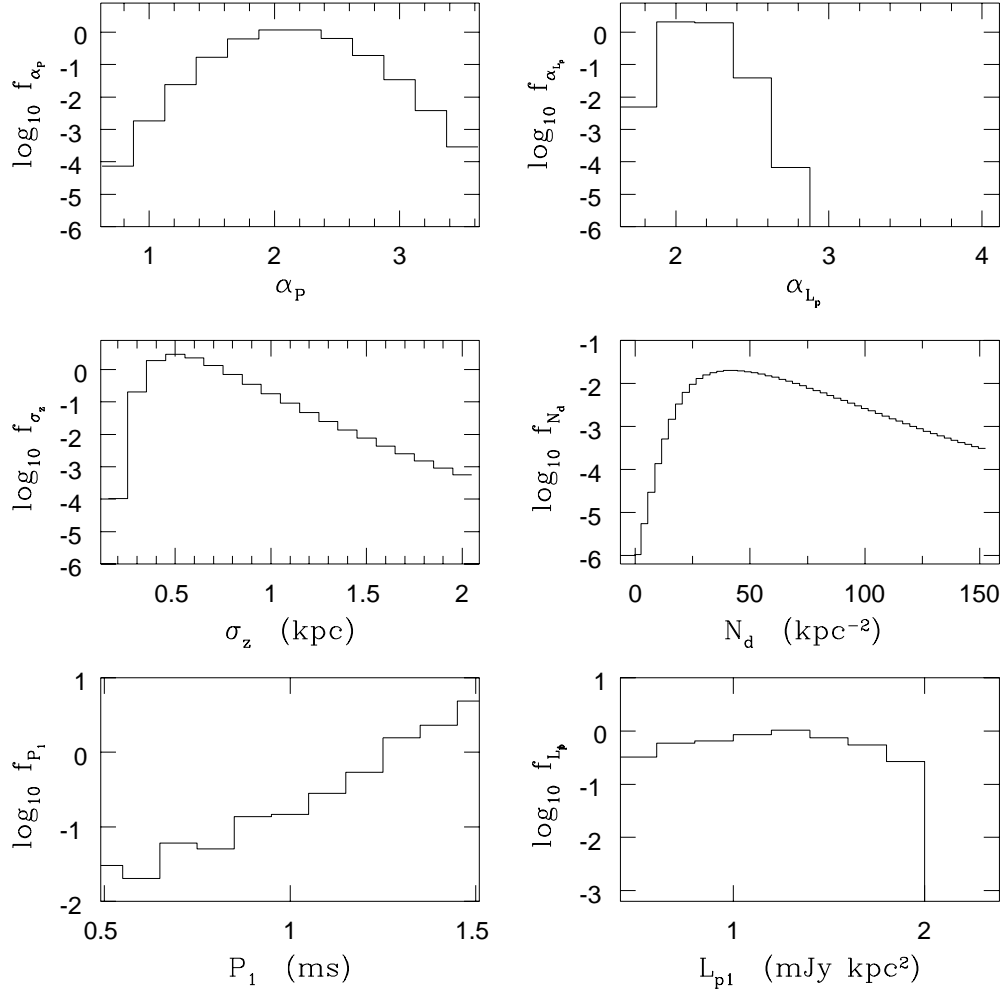


Fig. 5.— Marginal pdfs for the 6 parameters of the exponential disk model for the millisecond population. N_d is the column density (kpc^{-2}) of MSPs, which we show instead of the number density, n_d .

not occur and we discuss the significance of the cutoff P_1 next.

The specific value of P_1 depends, of course, on our assumption of a power-law distribution for P . We have not explored other mathematical forms, but reasonable alternatives include a power law that flattens for periods less than some critical period and cuts off at P_1 or a distribution that rises slowly from zero at P_1 and peaks at or near 1.56 ms and then follows a power-law form like that we have fitted. It is easy to see that such alternative period distributions will lead to *smaller* P_1 than we have derived. The reason is that they imply that smaller volume has been surveyed for $P < 1.56$ ms, so the allowed P_1 can be smaller. Therefore, our derived P_1 using the power-law distribution is a maximally allowed value and suggests, conservatively, that the period range for MSPs may extend to as small a value as 1 ms (95% confidence) or 0.65 ms (99% confidence).

Harding (1984) analyzed the slope of f_P , assuming a steady-state flux with births balanced by pulsars crossing the Hubble line. She showed that if pulsars are born with a powerlaw distribution of B ($\propto B^\beta$) and with initial period P approximately $\propto B$ (accretion spin up models imply $B^{6/7}$) then the resultant $f_P \propto P^\beta$. Today it is known that the spin-down times for the observed MSPs are too long for a steady-state to be attained. However, with similar assumptions we find the same slope in the period range $[P_{min}(T_h), P_{max}]$, where $P_{min}(T_h)$ is the period reached after a Hubble time (T_h) by the minimum initial period object (minimum magnetic field) and P_{max} is the longest period at birth. (Different slopes are found in other period subintervals. Additional discussion will be found in Chernoff & Cordes 1996a). Thus, one possible interpretation of the steep period slope is that the field distribution $\propto B^{-2.0 \pm 0.33}$. However, it is difficult to derive robust constraints on the field distribution without knowing both the time dependence of magnetic fields during the spinup process and the spindown law for MSPs subsequent to the spinup phase.

5.2.2. Scale Height σ_z

The inferred Gaussian scale (0.65 kpc) and exponential scale (0.50 kpc) are in rough agreement. The values indicate that the MSPs have a relatively small scale height, comparable to the oldest disk stars. Though the confidence intervals overlap, the actual shape of the distribution plays some role in the value of the scale height parameter and motivates, in part, a more physical analysis based on motion of objects in the Galactic potential (§6).

5.2.3. Minimum Luminosity L_{p1} and Slope α_{L_p}

The luminosity pdf of our best fit, $dN/dL_p \propto f_{L_p}(L_p) \propto L_p^{-2 \pm 0.2}$, is similar to that of long-period pulsars (e.g. Lyne, Manchester & Taylor 1985). Total numbers are dominated by weak sources. The lower cutoff is $L_{p1} = 1.1_{-0.5}^{+0.4}$ mJy kpc $^{-2}$ and is largely determined by the absence of nearby sources. We have shown for long-period pulsars that f_{L_p} is strongly influenced by geometrical beaming effects, the distribution of true luminosities, the spin down law and a

death line (Chernoff & Cordes 1996a). Because all four of these elements may differ between high-field pulsars and MSPs, we currently regard the similarity between the long-period and MSP luminosity distributions as fortuitous.

In the past, the disk-determined $f_{L_p}(L_p)$ (slope and cutoff) has also been used to make inferences about the number of MSPs in globular clusters. On evolutionary grounds, many properties of disk and globular cluster MSPs might be expected to differ (e.g. distributions of luminosity, spin period, orbital period and velocity). Since the nearest cluster is too distant to allow direct measurement of the luminosity function near L_{p1} , usage of the disk-determined form is necessary for many purposes. Fruchter & Goss (1990) measured the radio flux from nearby globular clusters and estimated $\sim 10^3$ MSPs in the Galaxy’s globular cluster system. Our best fit luminosity distribution, with cutoffs, is consistent with the one they assumed and does not alter the size of this estimate. Likewise, estimates by Foster & Tavani (1992) and Johnston, Kulkarni & Phinney (1992) of the *shape* of the luminosity pdf for MSPs in globular clusters are also consistent with our best-fit f_{L_p} for disk MSPs, though both groups were unable to determine the lower luminosity cutoff and, hence, the absolute normalization. Wijers & van Paradijs (1991) find far fewer globular cluster MSPs than do Fruchter & Goss or Johnston, Kulkarni & Phinney even though they adopted a lower luminosity cutoff three times smaller than that of Fruchter & Goss; the difference is probably related to their assumed dependence of luminosity on spin period and spin period derivative that was based on young, high-field pulsars. Analysis of globular cluster MSP populations should probably use a treatment similar to this paper’s but applied to cluster-only data.

5.2.4. Correlations

Most of the derived parameters are uncorrelated. However, α_P and P_1 are positively correlated as are α_{L_p} and L_{p1} , while n_d is negatively correlated with the lower cutoffs in period (P_1) and luminosity (L_{p1}). Figure 6 shows contours of constant likelihood plotted against pairs of parameters while holding all other parameters fixed at values that yield the maximum likelihood.

6. DYNAMICAL MODELS

6.1. Birth Kick Determination

In §5 we assumed functional forms for the z distribution of MSPs and fit for the associated scale height parameters. These parameters describe the present-day MSP distribution without regard to the orbit about the Galaxy. We have constructed a dynamical model that connects “birth parameters” to today’s spatial distribution as follows. We model the birthrate density of

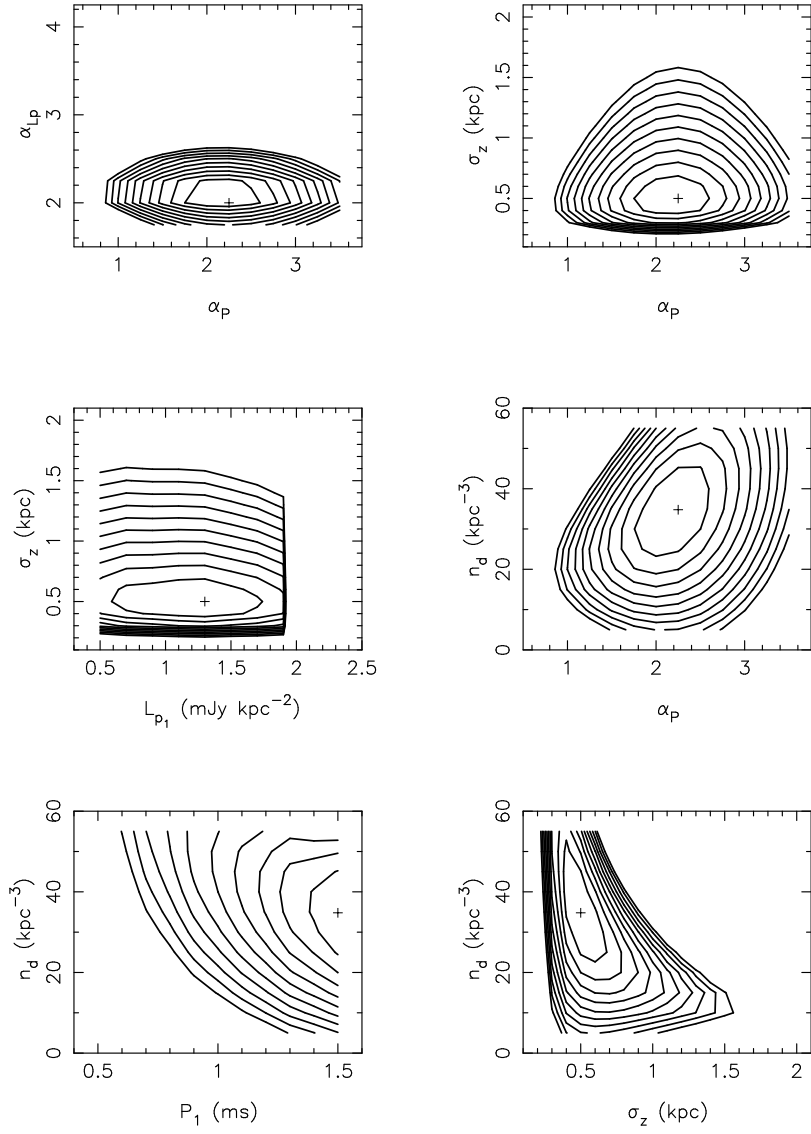


Fig. 6.— Selected contour plots of the log likelihood for the exponential model plotted against pairs of parameters while holding the other four parameters fixed at their values that yield the maximum likelihood. Contour spacings are unity in natural log units and the first contour is a factor 1/e from the peak.

MSPs

$$\dot{n}(R, z) = g(R) \exp\left(-\frac{z^2}{2\sigma_{z,b}^2}\right), \quad (29)$$

where R is (cylindrical) Galactocentric radius, z is height about the plane, $\sigma_{z,b}$ is a scale height parameter and $g(R)$ is a surface density function, taken to be either constant (“uniform model”) or exponential with scale length 3.5 kpc (“exponential model”).

The birth velocity is the circular rotation velocity plus a kick component. Note our use of “kick” includes *any* momentum impulse imparted to the pulsar’s progenitor or companion, if in a binary. The angular distribution of the kick is isotropic and the velocity magnitude has a distribution $\propto V^2 e^{-V^2/2\sigma_V^2}$. After birth, the MSP trajectory is determined by integration of the orbit about the Galaxy in a simplified model of the gravitational potential (Paczynski 1990). We ignore the role of scattering from irregularities (e.g. GMC’s, spiral density waves, massive black holes) in the calculated motion. We first discuss the kinematic properties of the MSP population inferred from the smooth model and next assess the degree to which our conclusions may be modified by the diffusion of stellar orbits.

About 4 million orbits were integrated over time spans of 10^9 years, sufficiently long that the derived vertical distribution was stationary and well-mixed. For specific birth parameters, the vertical distribution of MSPs in the vicinity of the Sun (e.g. in an annulus of Galactocentric radii from 7.5 – 9.5 kpc) was calculated by appropriately weighting and combining the results for the individual orbits.

The statistical analysis described in previous sections was carried out to determine the birth parameters (σ_V and the intrinsic pulsar population parameters) of the uniform model. The results (Table 3) give a peak value $\sigma_V = 52^{+17}_{-11}$ km s $^{-1}$. The initial scale height is not well-determined by the data and was held fixed, $\sigma_{z,b} = 0.1$ kpc. The column density of MSPs was calculated from Eq. 25. The result is consistent with values obtained using the Gaussian and exponential spatial models. Figure 7 illustrates the density distribution vs. z , comparing the range of allowed exponential fits (§5) to the most likely dynamical model. The differences are subtle and suggest that the assumed exponential form should be an adequate local description for many purposes.

6.2. Kinematics of Today’s Population

Kinematic properties of the MSP population may be inferred from the dynamical model. For example, the distribution of parallel and perpendicular velocities relative to the LSR are easily derived from the orbital calculations. Figure 8 shows the distributions for all simulated objects within 1 kpc of the Sun for the most likely dynamical model. The expected transverse motions are small; approximately 99% of the MSPs have $\Delta V_\perp < 150$ km s $^{-1}$. As MSP samples increase in number, detailed distributions like these will provide important additional constraints on modeling.

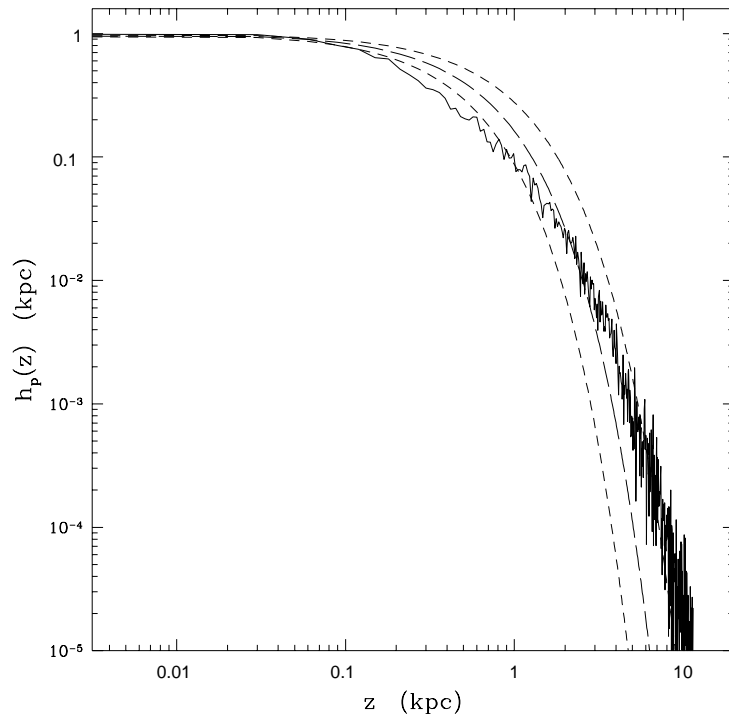


Fig. 7.— Comparison of the z distributions for the best fit velocity model (noisy solid line) and three exponential models with scale heights of 0.41, 0.55 and 0.78 kpc (dashed lines).

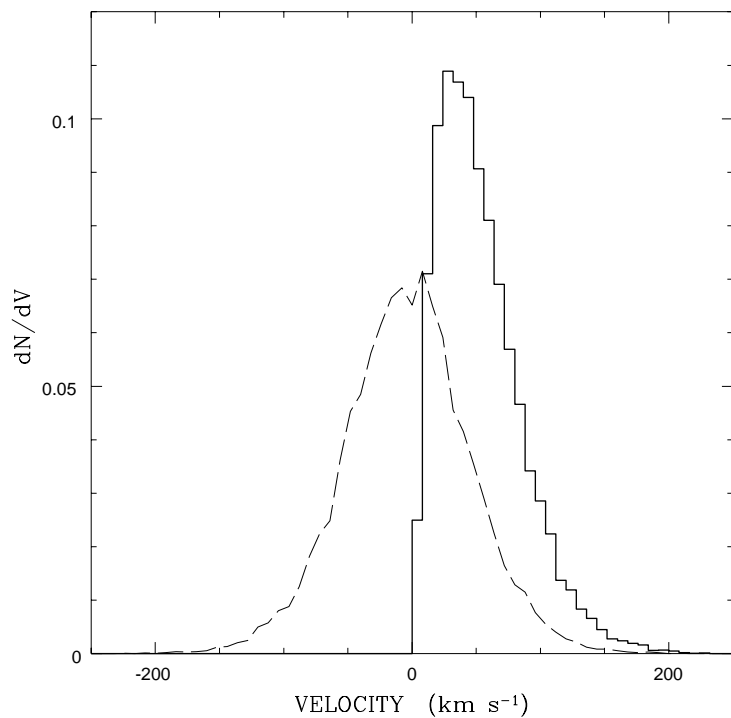


Fig. 8.— Histograms of observed transverse speeds (solid) and line-of-sight (dashed) velocity for the best fit velocity model of §6.

Next, we consider the velocity ellipsoid of MSPs. Let v_R , v_t and v_z be the components of velocity in the cylindrical radial direction, in the tangential direction (parallel to the local circular velocity, e.g. $l = 270^\circ$ at the solar position) and out of the plane, respectively. In the well-mixed state, the most interesting non-zero moments are $\langle v_R^2 \rangle$, $\langle v_t^2 \rangle$, $\langle v_z^2 \rangle$ and $\langle v_t \rangle$. Table 5 lists the first and second moments for a range of MSP birth models with $\sigma_V = 20, 40, 60, 80$ and 100 km s^{-1} , for two scale heights $\sigma_{z,b} = 0.05$ and 0.15 kpc , and for the uniform and exponential surface density distributions. (All velocity moments are given in units of σ_V .) When the kick velocity is small compared to the rotation velocity and when disk properties do not vary significantly over the range of radii sampled, the results of epicyclic theory are directly applicable. For local objects $\langle v_t^2 \rangle / \langle v_R^2 \rangle = |B/(A - B)|$ has the observed value 0.45 ± 0.09 (for Oort constants $A = 14.5 \pm 1.5 \text{ km s}^{-1} \text{ kpc}^{-1}$ and $B = -12 \pm 3 \text{ km s}^{-1} \text{ kpc}^{-1}$ [Binney & Tremaine 1987]). The model-calculated value of 0.45 at $\sigma_V = 20 \text{ km s}^{-1}$ is in good agreement with the value inferred from the observed Oort constants. Here, we will concentrate on the changes that occur as σ_V increases and that are indicative of some of the differences between the velocity distributions of MSPs and of disk stars. A global model is necessary since a local epicyclic treatment for the MSPs is not well-founded. For example, with a kick of 60 km s^{-1} particles observed at the local position could come from initial radii in the approximate range $(0.5 - 2.6) \times R_0$, where R_0 is the Sun’s distance from the Galactic Center. Also, kicks of this size create vertical excursions of $> 0.3 \text{ kpc}$, spoiling a harmonic approximation to the potential.

Table 5 shows how the basic moments change as σ_V increases. We briefly note the most important conclusions: (1) A clearly noticeable effect is the occurrence of a non-zero tangential motion measured with respect to the local circular velocity (“asymmetric drift”). For $\sigma_V = 60 \text{ km s}^{-1}$ the magnitude is $\sim 13 \text{ km s}^{-1}$ in the uniform model ($\sim 25 \text{ km s}^{-1}$ in the exponential model), an effect that is potentially detectable in a relatively small sample of objects with well-determined velocities. (2) The velocity ellipsoid (with axial ratios $\sqrt{\langle v_R^2 \rangle} : \sqrt{\langle v_t^2 \rangle} : \sqrt{\langle v_z^2 \rangle}$) becomes rounder as the magnitude of the kick grows. (3) The birth distribution in Galactocentric radius affects the value of all the non-zero velocity moments including the shape of the velocity ellipsoid and the magnitude of the asymmetric drift. (4) The imprint of the birth scale height is essentially absent for objects with $\sigma_V \gtrsim 60 \text{ km s}^{-1}$.

Determinations of asymmetric drift would provide valuable information on the birth locations of MSPs. Proper estimation of the effect will require more field MSPs than are currently known and careful treatment of distance errors. We defer a detailed discussion to another paper.

6.3. Orbital Diffusion

The model calculations presented above assume a regular background potential. Older stars are well known to have larger velocity dispersions, presumably from interaction with small-scale fluctuations in the gravitational field, but the actual physical source of the irregular field is not

well understood (Wielen 1977). The oldest stars, K and M giants of age 9×10^9 yrs, reach total dispersions of 77 km s^{-1} ; for comparison, using interpolated values for the uniform model in Table 5 we estimate that the best fit model for the MSPs ($\sigma_V = 53 \text{ km s}^{-1}$) implies a total dispersion of 84 km s^{-1} . In fact, the MSPs suffer comparable energy input from kicks and from diffusion. The key assumption is that the MSP population includes members with ages ranging uniformly up to the age of the Galaxy, so that the average effect of diffusion will be less than it is for the oldest stars. Using the velocity dispersion data of K and M giants with ages $(0.3 - 9) \times 10^9$ (Wielen 1977), averaging uniformly in time, we infer that the root mean square dispersion is $\sim 50 \text{ km s}^{-1}$. We suggest that the residual dispersion of 67.5 km s^{-1} (i.e. $\sqrt{84^2 - 50^2}$) is due to kick(s) unique to MSP evolution. This 3D dispersion would then correspond to a 1D kick of $\sim 39 \text{ km s}^{-1}$.

6.4. Conclusions

The best fit uniform model implies $\sigma_V = 53 \text{ km s}^{-1}$; this is an upper limit because gravitational scattering processes are ignored in its estimate; the scale of the kick is $\sim 40 \text{ km s}^{-1}$ assuming MSPs are long-lived and born at a uniform rate. If MSPs are visible for less than a Hubble time, the kick size will increase; if most of today's MSPs were formed early in the Galaxy's life, the kick size will decrease.

7. DISK + DIFFUSE MODEL

7.1. Method

The MSP distribution may be more complex than a single disk component with small scale height. For example, there may exist a population of MSPs that fill a halo-like region around the disk.

If MSPs are distributed in two components, the log likelihood becomes

$$\Lambda(\boldsymbol{\theta}, n_d, n_h) = -[n_d V_d + n_h V_h] + \sum_{k=1}^{M_p} \ell n \left[n_d \delta V_p^{(d)} + n_h \delta V_p^{(h)} \right]. \quad (30)$$

Here, we label disk quantities with 'd' while 'h' denotes diffuse (halo-like) contributions; we suppress the dependences of the volumes on other parameters. Maximizing Λ with respect to n_d and n_h , we find that the best-fit number densities \hat{n}_d and \hat{n}_h satisfy

$$\hat{n}_d V_d + \hat{n}_h V_h = M_p. \quad (31)$$

Also, if we take the $n_h = 0$ case as a fiducial solution, which is our result in §5 for the disk-only

model, the log likelihood for $n_h \neq 0$ may be expanded as

$$\Lambda(\boldsymbol{\theta}, n_d, n_h) = \Lambda(\boldsymbol{\theta}, n_d, 0) - n_h V_h + \sum_{k=1}^{M_p} \ell n \left(1 + \frac{n_h \delta V_p^{(h)}}{n_d \delta V_p^{(d)}} \right). \quad (32)$$

7.2. Diffuse Models

One might expect a diffuse distribution of MSPs for any of several reasons. (1) The probability distribution of birth velocities may extend to values much larger than typically allowed by the assumed Gaussian or exponential forms. The high velocity MSPs would oscillate to higher z distances or escape the Galaxy all together. (2) MSPs born in globular clusters may be ejected by dynamical interactions or when a cluster is tidally dissolved. Such objects would have a spatial distribution like the parent systems assuming the ejection velocities were small compared to the rotation velocity. (3) Spheroid stars may evolve and produce long-lived MSPs just like disk stars (e.g. by accretion-induced spinup). Such objects would have a spatial distribution like the Pop II spheroid. (4) If the formation of the Galaxy involved hierarchical merging of smaller objects containing disk-like structures, their MSPs will be cannibalized. Such objects might follow the dark matter halo distribution.

Without further considering the merits of these basic scenarios, we will adopt several geometrical distributions for the putative diffuse population and place upper limits on the number densities. Consider a density model for MSPs of the form

$$n_h(r) = n_h \left[1 + (r/r_h)^2 \right]^{-s_h/2}, \quad (33)$$

where r is the radius from the center, r_h is the characteristic radius, and s_h is the power-law index. Taking $s_h = 0$ gives a uniform density halo, our reference model (in practice all distributions are truncated at 50 kpc). Taking $s_h = 2$ and $r_h = 5$ kpc gives an isothermal distribution with large core. Taking $s_h = 3.5$ and $r_h = 1$ kpc gives the observed globular cluster distribution (Thomas 1989).

Using these models, we calculate the diffuse pulsar density by integrating Eq. 7 and we evaluate the halo volume factors V_h and $\delta V_p^{(h)}$ (Eqs. 17 and 19). We combine these with the analogous disk quantities and examine a grid in n_d and n_h to find the distribution of likelihood values.

7.3. Results

For our reference model, we find that the pure disk model is favored by a huge factor implying an upper bound on the diffuse density from the fitting is $n_h \lesssim 0.4$ kpc⁻³ (90% confidence, cf.

Table 4). Figure 9 shows likelihood contours for the disk and diffuse densities, with a maximum at $n_h = 0$. The marginalized densities are shown in Figure 10 for the uniform density model.

For the other two models, we have expressed the results in terms of limits on the density parameter n_h (the value at the center of the Galaxy) and, equivalently, on $n_h(R_0)$ where R_0 is the Sun’s galactocentric radius. Though we have made calculations explicitly for the nonuniform density models, the local values are close to the reference model values. This follows because on the Galactic scale most surveys probe regions near the solar system.

7.4. Disk, Spheroid, Halo and Globular Cluster Contributions

The local column density of MSPs, $N_d \sim 50_{-20}^{+30} \text{ kpc}^{-2}$, may be combined with the disk surface mass density ($\sim 66 \pm 8 M_\odot \text{ pc}^{-2}$ for Oort K giants, Bahcall 1984) to infer that the number of MSPs per unit disk mass $(dN/dM)_{disk} \approx 7.6_{-3.1}^{+4.4} \times 10^{-7} M_\odot^{-1}$ (the range reflects only the uncertainty in N_d). The total number of MSPs in the Galactic disk scaled to the disk mass M_{disk} is $3.0_{-1.2}^{+1.8} \times 10^4 (M_{disk}/4 \times 10^{10} M_\odot)$ (for example, $M_{disk} = 3.7 \times 10^{10} M_\odot$ [Bahcall & Soneira 1982] by one estimate; $(3.5 - 4.6) \times 10^{10} M_\odot$ [Caldwell & Ostriker 1981] by another). The total does *not* include a correction for beaming.

Estimates of the local spheroid mass density are uncertain, e.g. $\rho_{sph} = 1.88 \times 10^{-4} M_\odot \text{ pc}^{-3}$ (Bahcall, Schmidt & Soneira 1982) or $\rho_{sph} = (1.11 - 1.25) \times 10^{-3} M_\odot \text{ pc}^{-3}$ (Caldwell & Ostriker 1981). If $(dN/dM)_{disk} = (dN/dM)_{sph}$, then the spheroid makes a contribution to the MSP number density $n_{sph} = 0.14 \text{ kpc}^{-3}$ or $(0.84 - 0.95) \text{ kpc}^{-3}$, respectively. The upper limit we have derived for a uniform density model, $n_h \lesssim 0.42 \text{ kpc}^{-3}$, is marginally consistent. Future observations should be able to constrain contributions to the MSP population from Population II progenitors more strongly.

Estimates of the dark matter halo density are $\rho_{halo} = 9 \times 10^{-3} M_\odot \text{ pc}^{-3}$ (Bahcall, Schmidt & Soneira 1982) or $\rho_{halo} = (5.9 - 10.2) \times 10^{-3} M_\odot \text{ pc}^{-3}$ (Caldwell & Ostriker 1981). If the dark matter halo component satisfied $(dN/dM)_{disk} = (dN/dM)_{halo}$ then its contribution is $n_{halo} = 6.8 \text{ kpc}^{-3}$ or $(4.5 - 7.7) \text{ kpc}^{-3}$, respectively. Our limit on n_h implies $(dN/dM)_{halo}/(dN/dM)_{disk} < 0.06$ or $(0.05 - 0.09)$, respectively.

Today’s globular clusters are known to have a significant enhancement of MSPs relative to the disk. With considerable uncertainty, Phinney and Kulkarni (1994) estimate $(dN/dM)_{gc} \approx 50(dN/dM)_{disk}$. If half of the original globular cluster system has been destroyed (e.g. a total mass $M \approx 5 \times 10^7 M_\odot$), if the MSP content was similarly enhanced and if these MSPs orbit like the observed clusters, then the contribution to the local mass density is $1.1 \times 10^{-3} M_\odot \text{ kpc}^{-3}$ and the MSP number density is $4.2 \times 10^{-2} \text{ kpc}^{-2}$. Our limit on n_h does not provide a strong constraint.

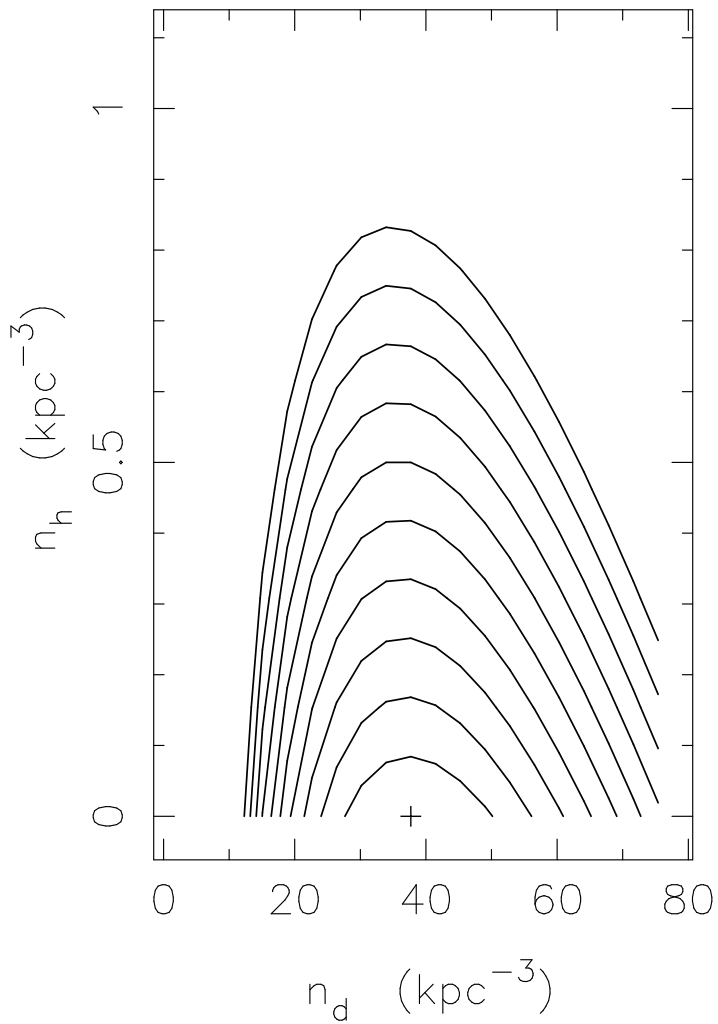


Fig. 9.— Contours of log likelihood plotted against the densities of MSPs in disk (n_d) and diffuse (n_h) components. The plot is for a uniform halo that extends well past the solar circle. Contour spacings are unity in the natural log. The plus sign marks the peak likelihood.

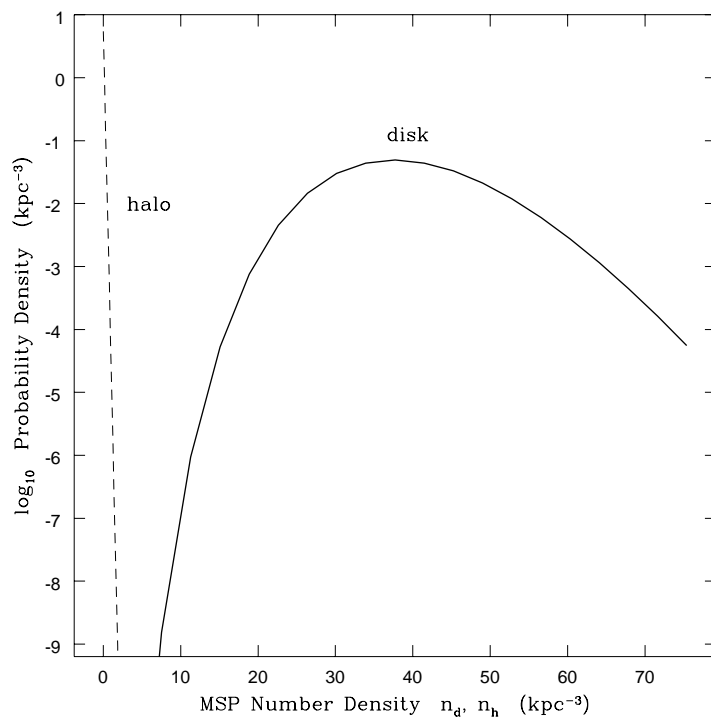


Fig. 10.— Marginal probability density functions for the disk and diffuse MSP densities, n_d and n_h , respectively.

7.5. Conclusions

The observations place an upper limit on a diffuse halo-like contribution to the MSP density that is roughly 1% of the MSP disk density at midplane.

8. SPACE VELOCITIES OF MSPS

Our results indicate that millisecond pulsars are a low-velocity population, at least when compared with young, high-field pulsars. We have found that the 3D rms velocity of MSPs in the galactic disk is $\sim 84 \text{ km s}^{-1}$, about a factor of 5-7 lower than that of young, strong field pulsars (Lyne & Lorimer 1994; Cordes & Chernoff 1996). We have reached this conclusion by determining the spatial distribution of MSPs, by excluding the existence of a significant non-disk population and by modeling the motion of objects in the gravitational potential of the Galaxy.

8.1. Comparison with Proper Motion Data

We may compare our results with direct measurements of proper motion using interferometric and pulse-timing methods; the indirect method of interstellar scintillation has also yielded determinations of MSP transverse speeds. To date, there are timing proper motions on eight MSPs: J0437-4715 (Bell *et al.* 1995), B1257+12 (Wolszczan 1994), J1713+0747 (Camilo, Foster & Wolszczan 1994), B1855+09 & B1937+21 (Kaspi *et al.* 1994), B1957+20 (Arzoumanian, Fruchter & Taylor 1994), J2019+2425 and J2322+2057 (Nice & Taylor 1995). There are also scintillation speeds on some of these and other pulsars, B1855+09 (Dewey *et al.* 1988), B1937+21 (Cordes *et al.* 1990), and J0437-4715, J1455-3330, J1730-2304 & 2145-0750 (Nicastro & Johnston 1995). These MSPs have transverse speeds that are less than 100 km s^{-1} , except for B1257+12, which has a speed of 285 km s^{-1} at its nominal distance of 0.62 kpc and B1957+20, which has $V_{\perp} \sim 173 \text{ km s}^{-1}$ at a distance of 1.2 kpc (Aldcroft, Romani & Cordes 1992). For the most part, these objects are consistent with our determination of the 3D rms velocity based on the locations of 22 MSPs and the absence of MSPs in substantial portions of the volumes searched in high-latitude surveys. However, the estimated transverse speed for B1257+12 is inconsistent with the overall distributions in z and velocity that we have derived, even though it was included in the fitting. One possibility is that its distance is overestimated, perhaps by as much as a factor of two, an amount sufficient to bring it into consistency with the statistical distribution. It is also possible that there are several evolutionary paths for producing MSPs (cf. §10), most of which produce low-velocity MSPs with others creating rarer, faster MSPs.

Further study of larger samples of MSP proper motions will result from a combination of new surveys, which will discover large numbers of MSPs (cf. §12), and use of timing and VLBI techniques. Use of the VLBA in conjunction with the Arecibo telescope and the Green Bank

Telescope should allow measurement of proper motions for dim and slow MSPs out to a few kpc.

9. BIRTH RATES OF DISK & HALO MSPS

For the disk-only model of §5, we have found the column density of MSPs with $P_1 = 1.56$ ms, $L_{p1} = 1.1$ mJy kpc $^{-2}$ for a plane-parallel model in z to be $N_d \approx 50^{+30}_{-20}$ kpc $^{-3}$ (Table 3). The implied number of MSPs in a disk of radius R_d with $P > P_1$ and $L_p > L_{p1}$ is

$$N_{MSP}(> P, > L_p) \approx 1.6^{+0.9}_{-0.6} \times 10^4 \left(\frac{R_d}{10 \text{ kpc}} \right)^2 \left(\frac{P}{1.56 \text{ ms}} \right)^{-1 \pm 0.33} \left(\frac{L_p}{1.1 \text{ mJy kpc}^{-2}} \right)^{-1 \pm 0.2}, \quad (34)$$

where the upper and lower values denote the 68% interval. Extrapolation on a per mass basis from the local disk surface density to a total disk mass, M_{disk} , implies

$$N_{MSP}(> P, > L_p) \approx 3.0^{+1.8}_{-1.2} \times 10^4 \left(\frac{M_{disk}}{4 \times 10^{10} M_\odot} \right) \left(\frac{P}{1.56 \text{ ms}} \right)^{-1 \pm 0.33} \left(\frac{L_p}{1.1 \text{ mJy kpc}^{-2}} \right)^{-1 \pm 0.2}. \quad (35)$$

These estimates do not include any correction for pulse beaming, whose influence is highly uncertain for MSPs. Estimates for this correction range from 1 to 3 (e.g. Bailes & Lorimer 1995). The totals are sensitive to the cutoff at small periods and at small luminosities.

The corresponding birthrate for MSPs, if constant over a galactic age 10^{10} yr, for the uniform disk

$$\dot{N}_{MSP}(> P_1) = 1.6^{+0.9}_{-0.6} \times 10^{-6} \text{ yr}^{-1} \left(\frac{R_d}{10 \text{ kpc}} \right)^2, \quad (36)$$

and for the extrapolated surface density is

$$\dot{N}_{MSP}(> P_1) = 3.0^{+1.8}_{-1.2} \times 10^{-6} \text{ yr}^{-1} \left(\frac{M_{disk}}{4 \times 10^{10} M_\odot} \right). \quad (37)$$

From our constraints on diffuse populations of MSPs, we conclude that, in the vicinity of the Sun, the MSP birth rate per unit volume is 100 times less than that from the disk.

9.1. Comparison with Other MSP Population Studies

Our estimates may be compared with those derived by Bailes & Lorimer (1995), Lorimer (1995) and Lorimer *et al.* (1995), who used the Vivekenand & Narayan scale-factor method to determine the number of MSPs in the Galaxy and the associated luminosity function. In their analyses, specific spatial distributions for the MSPs were adopted to derive the scale factors. BL assumed two different scale heights (0.3 and 0.6 kpc) along with a fixed radial distribution to estimate $10^{4.4}$ and $10^{4.6}$ MSPs, respectively, for $L_p > 2.5$ mJy kpc 2 and if all MSPs beam toward us.

Lorimer *et al.* (1995) use the radial distribution of Lorimer *et al.* (1993) (a Gaussian with radial scale of 4.8 kpc) and a Maxwellian velocity distribution with rms velocity = $\sqrt{3} \times 100$ km s⁻¹ to estimate $(1.3 \pm 0.2) \times 10^4$ MSPs in the Galaxy that are beamed toward us with $L_p > 10$ mJy kpc².

Lorimer (1995) deduced lower bounds on the scale height and mean 3D space velocity for MSPs of 0.5 kpc and 80 km s⁻¹, respectively. These bounds are consistent with our determinations.

The numbers of pulsars derived by BL and Lorimer *et al.* (1995) are greater than the estimate in Eq. 35 by a factor $\sim 2 - 3$ for a luminosity cutoff of 2.5 mJy kpc². Since most of the MSPs known are near the Sun (within 2 kpc) an extrapolation to the whole Galaxy is necessary. The radial distributions used by BL and Lorimer *et al.* effectively multiply the uniform disk model result by ~ 1.6 and match our own extrapolation (based on scaling up the local disk surface density to the given total disk mass in Eq. 35). The extrapolation introduces uncertainty but the differences accrue from the following factors. First, the z scale height implied by the Lorimer *et al.* velocity distribution is larger than that derived by us by about a factor of 2. Second, our inclusion of scintillation effects yields a search volume that is about 30% larger than otherwise. Third, Lorimer *et al.* include four long period pulsars in their analysis with $P > 295$ ms that we exclude from the MSP sample. Together these differences in the assumed spatial distributions and MSP samples explain the size of the differences in the estimated total number of MSPs in the Galaxy.

BL synthesized a luminosity function for MSPs after correcting the observed numbers of pulsars for the volume scale factors. Their luminosity function is consistent with a power-law slope of -2 (according to our definition of f_{L_p}) but with a roll-off below 10 mJy kpc². Our method is able to constrain the lower cutoff on the luminosity function because we evaluate our results at values for L_p other than those of actually detected pulsars.

Similarly, BL suggest that the period distribution decreases in going from 1 to 10 ms and roughly estimate that there can be no more than $10^{4.3}$ MSPs with periods with $P = 1$ ms. Our results suggest that the number of pulsars between 1 and 1.5 ms is approximately 50% of the number with $P > 1.5$ ms, or about 5000 pulsars.

10. RELATIONSHIP TO LOW-MASS X-RAY BINARIES

10.1. Scale Heights of LMXBs and MSPs

The evolutionary paths that lead to MSPs are poorly understood (for a review see Bhattacharya 1995). If all MSPs are “spun up” by mass transfer from a companion star during an LMXB phase, then the birth rate of LMXBs must exceed that of MSPs. Kulkarni and Narayan (1988) estimated that the birthrate of field LMXBs is about 1-10% of the birthrate of field MSPs for an assumed LMXB lifetime of 10^9 years. With a diminished LMXB lifetime (10^7 years), the

birthrates are brought into agreement. Our improved estimate of the total number of MSPs in the Galaxy does not significantly alter the rate mismatch nor its strong dependence on LMXB lifetime. However, our work of the last section does point out that the extrapolation from the local MSP population to that of the Galaxy is uncertain by a factor of $\sim 2 - 4$ (and an additional factor of $1 - 3$ for beaming). As we will argue below, the kinematic similarity of the LMXB and MSP population manifested in the observed scale heights is reasonably strong evidence of an evolutionary link; given the great uncertainty in LMXB lifetimes, the best evidence for a causal connection between the two populations is not found in the relative number but in the similar spatial distribution. In addition, a comparison of the scale height distribution of MSPs with that of LMXBs can place significant constraints on evolutionary scenarios leading to MSPs.

The galactic LMXB scale height derived from analysis of a flux-limited sample (Naylor & Podsiadlowski 1993) is (0.44-1.17) kpc. Alternatively, based on distance estimates to a subset of LMXBs, van Paradijs and White (1995) infer a scale height of 0.5 kpc and, furthermore, argue that the LMXBs are predominantly located at Galactocentric radii less than 5 kpc. Although the two vertical scales are comparable, the interpretations are quite different. Van Paradijs and White assume that the LMXBs have Pop II progenitors and that the scale height is set by large velocity kicks at birth (of order 400 km s^{-1}) and the local disk acceleration, which they argue is 2.5-4 larger in the relevant inner regions of the Galaxy than locally. This analysis ignores the finite birth scale height and the lifetime of the objects. Naylor and Podsiadlowski, on the other hand, infer that the LMXBs derive from Pop I stars and have a scale height perpendicular to the plane that is roughly like that of the observed thin disk (with a small additional kick), which has a nearly constant value.

Our *local* determination of the MSP scale height is (0.53-0.81) kpc, comparable with the above LMXB estimates. If MSPs are descendants of the LMXB phase and if the scale height increases with age, then the local MSP population should have a scale height greater than or equal to the LMXB value. If the kicks were as large as suggested by Van Paradijs and White, the minimum local scale height of the MSPs would be (1.25-2) kpc, clearly inconsistent with our results. In addition, our upper limit on the diffuse number density of pulsars suggests that the observed MSPs were born in the disk (Pop I). A consistent interpretation of the LMXB and MSP data is that both are Pop I and both are derived from a similar evolutionary channel.

10.2. Origin of MSP Space Velocities

In future work, we will discuss how the observed scale height of MSPs and the inferred z velocities ($\sim 50 \text{ km s}^{-1}$) place stringent constraints on the evolution of binary systems that lead to MSP formation. One of the main problems in understanding the LMXB evolution path is that the formation rate (10^{-6} yr^{-1}) in the Galaxy is so small that the pathway is *a priori* special. A proposed scenario is as follows (Webbink & Kalogera 1994). A binary composed of a massive star ($M_1 = 10 - 20M_\odot$) and a light companion ($M_2 < 0.12M_1$) with an initial orbital separation

less than about 1000 R_{\odot} will pass through an epoch of unstable mass transfer and common envelope evolution once the massive star begins to swell. The interaction ejects much of the envelope, drawing the pair to very small distances of separation. If the helium core of the primary is sufficiently massive it is able to continue to burn and collapse even after its outer hydrogen envelope has been removed. The resultant neutron star has an orbit far smaller than the size of the original giant primary, an essential requirement if an LMXB phase is to take place. Starting with the pre-supernova system we have analyzed how a tight binary is affected by a combination of (1) asymmetric SN kick, (2) impact of ejected shell and (3) dissipative processes in the eccentric, surviving binary.

Two effects sculpt the properties of the binaries that survive to give LMXBs and/or MSPs. The intrinsic kick given a neutron star by the supernova explosion unbinds loosely bound binaries while the impact of the supernova shell on the secondary is responsible for destroying and/or unbinding tight binaries. The surviving binaries occupy a relatively narrow range in pre-supernova orbital separation, primary and secondary masses and have a limited range of center of mass velocities. Most of this analysis is independent of the specific evolutionary pathway leading to the pre-SN progenitor. (We present the details of this analysis in Chernoff & Cordes 1996b.)

11. SELECTION EFFECTS AGAINST FAST BINARIES

Orbital motion causes MSPs in compact binaries to be missed in surveys that assume the pulse period to be constant rather than Doppler shifted (e.g. Johnston & Kulkarni 1991). All blind surveys for MSPs, including the 8 analyzed in this paper, make this assumption. One circumstance in which the results of previous sections may be altered is if the spin period and/or luminosity depend in some way on orbital period. For example, a relation between spin and orbital period might be expected on general evolutionary grounds for spun up MSPs (Alpar *et al.* 1982, Ruderman & Shaham 1983). Some observations suggest a weak positive correlation (Lundgren, Zepka & Cordes 1995) implying that the selection against detecting spin periods less than 1.5 ms may be stronger than we have estimated. Because the measured correlation is weak we believe that any modification to the distribution of spin periods on this account will be modest. In any case, fast binaries have been missed in MSP surveys and their ultimate detection can only increase our estimated space densities for MSPs.

We now give a brief account of survey sensitivity to binary orbital period. The observation time $T \lesssim 1$ min for most of the Arecibo surveys, so that orbital effects are negligible for $P_{orb} \gtrsim 1.^h6 P^{-3/4}$ (P in ms) for WD companions with $M_2 = 0.3M_{\odot}$. However, surveys 4,7 & 8 with $T \sim 3$ min are insensitive to orbital motion only for $P_{orb} \gtrsim 8.^h5 P^{-3/4}$. Weighted by volumes searched, the surveys with longer T contribute strongly to an overall selection against MSP binaries with short periods. Indeed, J0751+1807 with $P_{orb} = 6.^h3$ was discovered in survey # 4 in a single harmonic, the higher harmonics having been attenuated by orbital motion (Lundgren, Zepka & Cordes 1995). That yet-faster binaries with fairly massive WD companions exist is

certain because objects like J0751+1807 experience orbital decay due to gravitational radiation on less than a Hubble time. Indeed, if MSP-WD binaries achieve $P_{orb} \lesssim 8^h$ solely due to such inspiral, then it may be shown that the orbital period distribution $dN/dP_{orb} \propto P_{orb}^{-5/3}$. Overall, our conclusions are unaffected for MSPs in binaries with orbital periods $\gtrsim 6$ hr and with companion masses $\lesssim 0.3M_\odot$.

Proper consideration of orbital effects — and estimation of the MSP orbital period distribution — requires an analysis of search volumes as a function of orbital period and companion mass as well as spin period and luminosity. Such a study is beyond the scope of the present paper.

Future surveys made with greater sensitivities than heretofore using the upgraded Arecibo Observatory and the new GBT will be able to probe to greater distances while also circumventing orbital suppression of Fourier harmonics. Furthermore, algorithms that correct for orbital motion are becoming much more feasible with the prospect of computers with teraflops capability.

12. OPTIMAL SEARCHES FOR MILLISECOND PULSARS

The population distributions we have derived may be used to optimize new searches for MSPs. Search sensitivities (Appendix A) depend on sky background, dispersion and scattering as well as on the flux densities and periods of the MSPs. Consequently, the optimal search is frequency and telescope dependent. Here we illustrate the contributions from different effects by showing δV_s , the *search volume* (the volume searched in a beam area, averaged over P and L_p , Eq. 8) and the *detection volume*, δV_d , (the volume searched weighted by the dimensionless density of MSPs, Eq. 18). To calculate each we use the best-fit distributions for P and L_p for the exponential disk model of §5 and Table 3. By definition $\delta V_d \leq \delta V_s$: surveys that search much more deeply than the scale height of the MSP population yield $\delta V_d \ll \delta V_s$. For concreteness, we consider a survey conducted by telescopes like the under-construction Green Bank Telescope (GBT) and a hypothetical analog in the Southern hemisphere, in order that we may consider a full sky survey. We assume receiver and survey parameters such that the minimum detectable flux density is about 2 mJy when looking at high galactic latitudes and long periods.

Figure 11 shows δV_s and δV_d per square degree for a search at 430 MHz. Search volumes (top portion of figure) increase more or less monotonically with galactic latitude but level off for $|b| > 30^\circ$. The volume is smallest toward the galactic center where the sky background is high and dispersion and scattering effects are large. By contrast, the detection volume (bottom part of figure) is maximum for $|b| \sim 20^\circ$ and $|l| \gtrsim 50^\circ$ and corresponds to directions that allow the largest $\int_0^{D_{max}} dDD^2 n_p(D, \ell, b)$. The latitude constraint ensures that the search depth does not exceed the MSP scale height. The longitude restriction follows from the variation of the search volume in the plane. The detailed shapes of the contours are dependent on the survey frequency and duration (per direction) but suggest that future surveys which concentrate on low latitudes will maximize the number of new discoveries. However, deep high latitude surveys will better constrain the falloff

toward larger z of the disk population as well as place tighter constraints on or make detections of any *bona fide* diffuse or halo-population pulsars. For the hypothetical survey depicted in Figure 11, a total detection volume $\sim 13.3 \text{ kpc}^3$ is sampled, corresponding to discovery of $\sim 585^{+330}_{-210}$ disk MSPs. This number is for a uniform disk component; any galactocentric radial dependence, likely to increase the number of MSPs toward the inner Galaxy, will only increase the number of detected MSPs.

13. DISCOVERING FAST PULSARS

Our fitting indicates that available survey data already place useful constraints on the minimum spin period in the MSP population (cf. §5 and Table 3). The reason such constraints may be placed is found in Figure 3 which shows that, for periods less than 1 ms, a nonzero (though small) volume has been searched. Here we estimate how much additional volume must be searched in order to expect to find pulsars with $P_1 < P < P_{\text{fast}}$ where P_{fast} is the maximum period of interest.

Using Eq. 7 we derive an upper bound on the volume that must be searched (evaluated at the minimum MSP period, P_1), in order that we find pulsars with periods faster than P_{fast} . Since surveys at low periods do not see to large D_{max} , we assume that they do not see as far as the z scale height $\sim 0.5 \text{ kpc}$. Performing the integrals we may write

$$\langle N_p \rangle \gtrsim n_d (1 - P_1/P_{\text{fast}}) \left[\frac{1}{3} \Omega_b \langle L_p^{3/2} \rangle S_{\min}^{-3/2}(P_1) \right]. \quad (38)$$

Defining the term in square brackets as $V_S(P_1)$ and requiring $\langle N_p \rangle \sim 1$ to obtain a likely detection, we find an *upper bound* on the required search volume to be

$$V_S(P_1) = \frac{1}{n_d (1 - P_1/P_{\text{fast}})}. \quad (39)$$

Evaluating Eq. 39 for $P_{\text{fast}} = 1.5 \text{ ms}$ and $n_d \sim 44 \text{ kpc}^{-3}$, we find that, as a function of the minimum period, $V_S(P_1)$ ranges from $\sim 1/25 \text{ kpc}^3$ for $P_1 = 0.65 \text{ ms}$ (our 99% lower bound on P_1) to $\sim 1/3 \text{ kpc}^3$ for $P_1 = 1.4 \text{ ms}$. Comparison with Figure 3 shows that, for the luminosity assumed for that figure ($L_p = 16 \text{ mJy kpc}^2$), the Parkes survey (#7) yields search volumes at these P_1 that are comparable to those needed to yield a detection of a pulsar faster than 1.5 ms. However, the assumed L_p for the figure is larger than average and the Parkes survey observes to depths that, for some directions, exceed the z scale height. Consequently, it is not surprising that a pulsar faster than PSR B1937+21 ($P = 1.56 \text{ ms}$) has not been found. Nonetheless, future surveys should be able to probe this region of period space and either find fast pulsars or determine better the period cutoff to the MSP population. Our results indicate that deeper surveys at low galactic latitudes (e.g. $|b| \lesssim 10^\circ$) will yield the search volume needed to accomplish these goals.

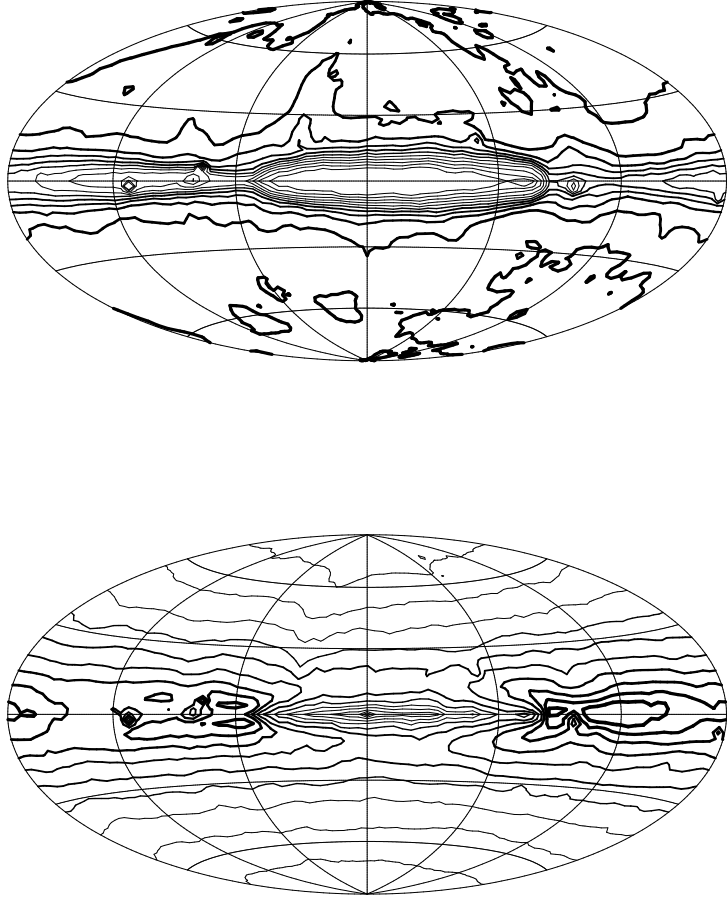


Fig. 11.— (Top:) Aitoff projection in galactic coordinates showing the *search volume* ($\text{kpc}^3 \text{ deg}^{-2}$) for a hypothetical full-sky survey at 430 MHz. The calculated volumes are averages over the period and luminosity distributions in our best-fit, exponential disk model. The minimum volume is toward the galactic center. The thinnest contour (toward the inner Galaxy) corresponds to the least volume ($10^{-3.6} \text{ kpc}^3 \text{ deg}^{-2}$) while the thickest line (at high latitudes) corresponds to the greatest volume ($\sim 10^{-1.9} \text{ kpc}^3 \text{ deg}^{-2}$). Most of the variation is from a deep minimum toward the Galactic center to a shallower variation beginning at $|b| \sim 15^\circ$. The greatest volumes searched are those toward the highest latitudes. Structure is seen in the plotted contours (e.g. the North Polar Spur) because the search sensitivity and, hence, depth are dependent on the sky background and on dispersion and scattering. (Bottom:) Similar projection for the *survey detection volume*. The minimum contour (toward the Galactic center) is $10^{-4.3} \text{ kpc}^3 \text{ deg}^{-2}$ while the maximum (thickest line) is $10^{-2.8} \text{ kpc}^3 \text{ deg}^{-2}$ at latitudes $|b| \sim 5^\circ$ and longitudes $|\ell| \gtrsim 50^\circ$. Note that there is no Galactocentric radial dependence of our assumed MSP number density, so all the structure at $b = 0^\circ$ (and other lines of constant latitude) is due to the depth of the survey.

14. DISCUSSION

Through a likelihood analysis, we have constrained the period and pseudo-luminosity distributions to be steep power laws with slopes ~ -2 . The distributions imply that the population of MSPs increases rapidly to smaller periods and smaller pseudo-luminosities. We infer a minimum period $P_{min} > 0.65$ ms at 99% confidence and a minimum luminosity cutoff $L_{p1} = 1.1^{+0.4}_{-0.5}$ mJy kpc 2 . The column density of MSPs in the local vicinity of the solar system is $N_d \sim 50^{+30}_{-20}$ kpc $^{-2}$. The limits on a diffuse halo-like component are $\lesssim 1\%$ of the midplane density. All these results are essentially identical for each of the models we have analyzed. Estimates of the total number of MSPs in the Galaxy are uncertain. Extrapolating on a per mass basis from the local disk surface density to a total disk mass, M_{disk} , we find $N_{MSP} \approx 3.0^{+1.8}_{-1.2} \times 10^4$ ($M_{disk}/4 \times 10^{10} M_\odot$) for cutoff period 1.56 ms and cutoff luminosity 1.1 mJy kpc $^{-2}$ (without correction for beaming).

Our analysis assumes specific forms for the period and luminosity distributions, namely power-law functions, that undoubtedly influence the specific values for numbers of pulsars in a given period range and also on the minimum period cutoff. We have not tested other mathematical forms for these distributions, so the true cutoff for the period distribution may be different than we have derived. Nonetheless, because the period distribution monotonically increases with decreasing period, our quoted minimum period is *larger* than it would be for a function that plateaus or decreases with decreasing period below 1.56 ms. We consider the most important implication of our derived minimum period to be that MSPs faster than those already found may indeed be present in the Galaxy: the surveys done heretofore cannot rule out their existence. In addition, modeling of the spinup process using full general relativity (Cook *et al.* 1994a,b) implies that gravitational instabilities do not prohibit the formation of very fast MSPs. Of course the ultimate existence proof for MSPs with $P < 1.56$ ms lies in future surveys that can explore large volumes of the Galaxy at these small periods. Such surveys will be feasible with new spectrometers that can sample more frequency channels at faster rates and with post processing that can contend with motion of fast pulsars in binaries.

Another implication of our results on the period distribution is that, if MSPs exist due to accretion-driven spinup of neutron stars, then accretion must ensue for sufficiently long times that periods shorter than 1.56 ms can be achieved. From the work of Cook *et al.* (1994a,b), such accretion appears possible without requiring typical ages for LMXBs that are so long as to resurrect the discrepancy between birth rates for MSPs and LMXBs.

The observed scale height of MSPs implies that they are a low-velocity population among neutron stars, having an rms speed that is about a factor of 5 smaller than that of young pulsars with much stronger magnetic fields. A part of the total inferred dispersion we attribute to a kick unique to the evolution of MSP systems (~ 40 km s $^{-1}$) and the rest to the effect of diffusive processes that increase the dispersion of old objects. A number of kinematic signatures that should be evident in larger MSP samples (transverse motions, asymmetric drift, shape of velocity ellipsoid) are described.

The disparity in velocity between the low-field MSPs and high-field pulsars might be taken as evidence that the two empirical classes of neutron stars are born through substantially different processes. If MSPs are produced largely through accretion-induced collapse of a white dwarf and if that process yields only a small kick to the resultant NS compared to Type II supernova then the observed dispersions of MSPs and high-field pulsars may find a natural explanation. In any case, the similarity in scale height of MSPs and LMXBs shows that the formation of the NS in both objects is accomplished without substantial center-of-mass impulses and supports the notion of an evolutionary connection. On the other hand, if binary survival after the type II supernova is the most significant bottleneck in the production of LMXBs and their MSP descendants, it is possible that the processes that dictate survival of the binary system are also responsible for allowing only a limited range of center-of-mass velocities. Correlations between spin and orbital periods and space velocity, such as those suggested by Bailes *et al.* (1994), depend critically on the details of mass transfer and on the number of evolutionary paths that lead to MSP formation. Elsewhere, we will present our detailed analysis of the effects that sculpt binary survival.

We thank Z. Arzoumanian, M. Bailes, G. Cook, D. Lorimer, T. Loredo, S. Lundgren and I. Wasserman for useful discussions. This work was supported by NSF Grants AST-91-19475, AST-95-30397, AST-92-18075 and NASA Grants 2581 and 2224 to Cornell University. It was also supported by the National Astronomy and Ionosphere Center, which operates the Arecibo Observatory under a cooperative agreement with the NSF.

APPENDICES

A. SEARCH SENSITIVITIES

The pulsar searches we consider involve the removal of dispersion delays between the outputs of a multichannel receive using trial values for the dispersion measure. The resultant time series is then Fourier analyzed. Suppose an N_{FFT} -length Fast Fourier Transform (FFT) is calculated from the time series for each trial dispersion measure. With a sample time Δt and pulse period P , harmonics appear in frequency bins

$$k_\ell = \frac{\ell \Delta t N_{FFT}}{P}, \quad \ell = 0, 1, \dots \quad (\text{A1})$$

including a “DC” term ($\ell = 0$) and the fundamental ($\ell = 1$). Let the intrinsic pulse shape be $s(t)$, $0 \leq t \leq P$ so that a (short) discrete Fourier transform (DFT) of this shape over a single pulse period is $\tilde{s}(\ell)$, $\ell = 1, \dots, M$. This function would determine the envelope of harmonic amplitudes in the long FFT were it not for additional contributions that derive from the post-detection averaging time (or “time constant”), from dispersion smearing across individual frequency channels, and from pulse broadening due to interstellar scattering (for distant sources). In many surveys, post-detection smoothing is simply an RC filter whose time domain response is a one-sided exponential function. Interstellar scattering produces nearly the same kind of time response, while the dispersion time function is dictated by the shapes of receiver filters, usually approximately Gaussian in form. Letting the M -point DFTs of the time constant, dispersion, and scattering functions be \tilde{s}_{tc} , \tilde{s}_d and \tilde{s}_s , respectively, we may write the effective envelope function of harmonics as

$$\tilde{s}_{eff}(\ell) = \tilde{s}(\ell) \tilde{s}_{tc}(\ell) \tilde{s}_d(\ell) \tilde{s}_s(\ell). \quad (\text{A2})$$

It is useful to define the ratio of the ℓ -th harmonic to the DC value as

$$R_\ell \equiv \left| \frac{\tilde{s}_{eff}(\ell)}{\tilde{s}_{eff}(0)} \right|. \quad (\text{A3})$$

Survey FFTs are analyzed by constructing partial sums of harmonics (of the FFT magnitude or squared magnitude) for different trial periods. These sums are typically of $N_h = 1, 2, 3, 4, 8$ and 16 harmonics, though there are variations on this. Suppose that a threshold η_T is chosen that represents the number of standard deviations in the FFT’s magnitude. This is typically $\eta_T \sim 6$ to 9 in order to minimize false-alarm rates when testing large numbers of spectral values (typically multiples of 10^9) in a survey.

The minimum detectable flux density for a sum of harmonics $1, \dots, N_h$ is

$$S_{min, N_h} = \frac{\eta_T T_{sys}}{G \sqrt{N_{pol} \Delta\nu \Delta t N_{FFT}}} \left(\frac{\sqrt{N_h}}{\sum_{\ell=1}^{N_h} R_\ell} \right), \quad (\text{A4})$$

(where T_{sys} is the system temperature [K]; G is the telescope gain [K Jy $^{-1}$]; $N_{pol} = 2$ is the number of independent polarization channels included; $\Delta\nu$ is the total bandwidth; and Δt is the sample interval). For searches that analyze $|\text{FFT}|^2$ rather than $|\text{FFT}|$, $R_\ell \rightarrow R_\ell^2$. The actual minimum flux density depends on the number of harmonics that contribute significantly which, in turn, depends on the duty cycle of the pulse. Because extrinsic effects (viz. dispersion and scattering), broaden the pulse, the optimal N_h and corresponding S_{min} are strongly dependent on the observation frequency, distance, direction and pulse period. The direction dependence is manifested in the dispersion measure to which a pulsar of given period may be detected. Consequently S_{min} is the minimum over all N_h considered in the analysis and may be written with dependences

$$S_{min} = S_{min}(\ell, b, P, DM, \nu, \Delta\nu, N_{ch}, T_{sys}, G, \dots). \quad (\text{A5})$$

In practice, surveys usually test only a subset of all possible harmonic sums. We take this into account when computing S_{min} for each survey.

Note that our expression for the minimum flux density differs from that often quoted in the literature (e.g. Camilo, Nice & Taylor 1996), which replaces the factor in large brackets in Eq. A4 with a factor $\sqrt{w/(P-w)}$, where w is the pulse width. The divergence of this factor as $w \rightarrow P$ is equivalent to *assuming* $R_1 = 0$, which overestimates the true S_{min} because, even when pulse smearing exceeds a pulse period, the variable flux remaining at the fundamental frequency can still be detectable for a luminous pulsar. Our expression takes this possibility into account, which corresponds to $0 < R_1 \ll 1$.

It is important to calculate accurately the minimum detectable flux density because it determines the galactic volume searched. This volume is small but not zero for very short periods $\lesssim 1.5$ ms.

B. INTERSTELLAR SCINTILLATIONS

Interstellar scintillations are intensity variations in both time and frequency caused by multipath propagation through ionized gas. At 400 MHz, both diffractive (DISS) and refractive (RISS) interstellar scintillations contribute to the flux variations of pulsars. Here we restrict the discussion to DISS, which will dominate RISS at 400 MHz and is especially important because its probability density is skewed whereas RISS is symmetric.

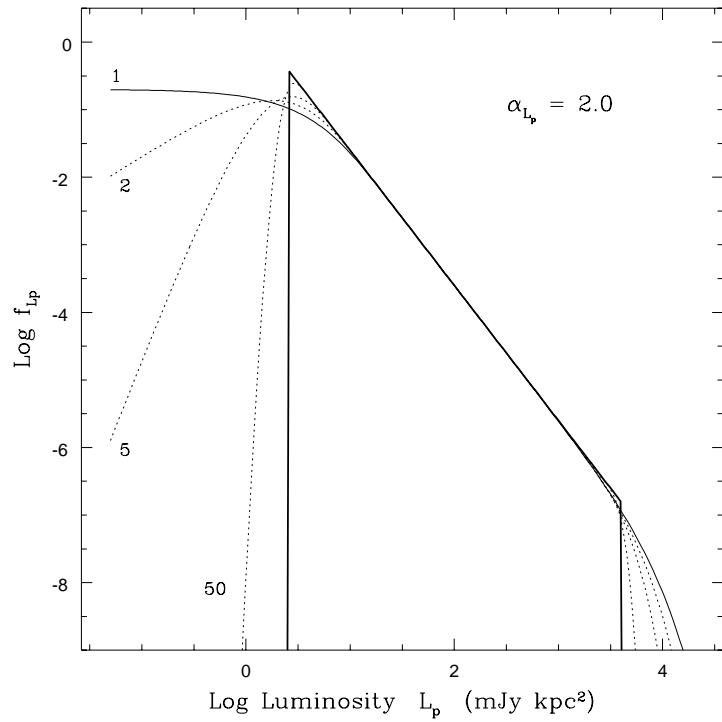


Fig. B1.— Luminosity functions with and without the effects of scintillations included. (Heavy Solid Line:) Intrinsic luminosity function having a power-law slope of -2 . (Light Solid Line:) The scintillated luminosity function when interstellar scintillations are saturated and unquenched by time-bandwidth averaging. (Dotted Lines:) Scintillated luminosity functions with various degrees of averaging, indicated by n_{iss} (cf. Eq. B3).

DISS causes the pulsar flux density S to vary as $S' = gS$, where g is the DISS gain that has a one-sided exponential distribution when DISS is saturated and not quenched by time-bandwidth averaging (Rickett 1990; Cordes & Lazio 1991). Except for the very nearest pulsars ($D < 100$ pc), DISS is saturated at 400 MHz. The characteristic time and frequency scales of DISS diminish with increasing distance. Use of finite bandwidth B and data-span length T will average over distinct scintillation maxima, increasing the number of degrees of freedom from 2 (for unquenched DISS) to $2n_{iss}$, where

$$n_{iss} \sim \left(1 + 0.2 \frac{B}{\Delta\nu_d}\right) \left(1 + 0.2 \frac{T}{\Delta\nu_t}\right), \quad (\text{B1})$$

$\Delta\nu_d$ is the characteristic bandwidth of DISS, and Δt_d is the characteristic time scale (Cordes 1986). The characteristic bandwidth and time scale have been measured for many pulsars and were used as input to the Taylor & Cordes (1993) model for pulsar distances. For our purposes, we use the TC model's estimation of the scattering measure along with the distance and frequency to estimate the scintillation parameters.

The pdf of g is

$$f_g(g, n_{iss}) = \frac{(gn_{iss})^{n_{iss}}}{g\Gamma(n_{iss})} e^{-gn_{iss}} U(g), \quad (\text{B2})$$

with $U(g)$ the Heaviside function and Γ is the gamma function. As $n_{iss} \rightarrow \infty$ (i.e. pulsars at large distances or observed at low frequencies), f_g tends toward a delta function, $\delta(g - 1)$.

We include scintillations in our analysis by defining a scintillated pseudo luminosity, $L'_p = gL_p$. For a luminosity function $f_{L_p}(L_p)$, the corresponding scintillated luminosity function is

$$f_{L'_p}(L'_p) = \int dg g^{-1} f_g(g, n_{iss}) f_{L_p}(L'_p/g). \quad (\text{B3})$$

The distinctive effect of DISS is that, if the intrinsic luminosity function has cutoffs at low and high luminosities, the scintillated luminosity function will not. In fact, the scintillated luminosity function will extend to zero luminosity because the most probable scintillation gain (for $n_{iss} = 1$) is zero. Luminosities larger than the upper cutoff will be seen owing to the long exponential tail of f_g (again for $n_{iss} = 1$). Figure B1 shows examples of scintillated luminosity functions for several values of n_{iss} . As $n_{iss} \rightarrow \infty$, the scintillated luminosity function tends toward the original, unscentillated luminosity function.

In surveys where DISS is saturated and unquenched ($n_{ISS} = 1$) and single trials are made on each sky position, the volume surveyed is effectively increased by a factor $\langle g^{3/2} \rangle = \Gamma(\frac{5}{2}) \sim 1.33$. Multiple trials can increase or decrease this volume factor, depending on how the results of the various trials are combined.

REFERENCES

- Aldcroft, T., Romani, R. W. & Cordes, J. M. 1992, ApJ, 400, 638.

- Alpar, M.A., Ruderman, M.A., Cheng, A.F. & Shaham, J. 1982, *Nature*, 300, 728.
- Arnaud & Rothenflud 1981, *A&A*, 103, 263.
- Arzoumanian, Z., Fruchter, A. & Taylor, J. H. 1994, *ApJL*, 426, L85.
- Backer, D.C. 1976, *ApJ*, 209, 895.
- Bahcall, J.N. 1984, *ApJ*, 287, 926.
- Bahcall, J.N. & Soneira, R.M. 1982, *ApJL*, 238, L17.
- Bahcall, J.N., Schmidt, M. & Soneira, R.M. 1982, *ApJL*, 258, L23.
- Bailes, M. *et al.* 1994, *ApJ*, 425, L41.
- Bailes, M. & Lorimer, D. 1995, in *Millisecond Pulsars: A Decade of Surprise*, Eds. A. S. Fruchter, M. Tavani & D. C. Backer, ASP Conference Series, 72, 17.
- Bell, J. F., Bailes, M., Manchester, R. N., Weisberg, J. M. & Lyne, A.G. 1995, *ApJ*, 440, L81.
- Bhattacharya, D. 1995, in *X-Ray Binaries*, Eds. W. H. G. Lewin, J. van Paradijs, & E. P. J. van den Heuvel, Cambridge Astrophysics Series, 26, 233.
- Bhattacharya, D. & van den Heuvel, E.P.J. 1991, *Physics Reports*, 203, 1.
- Binney, J. & Tremaine, S. 1987, *Galactic Dynamics*, Princeton University Press.
- Caldwell, J.A.R. & Ostriker, J.P. 1981, *ApJ*, 251, 61.
- Camilo, F., Foster, R. S. & Wolszczan, A. 1994, *ApJ*, 437, L39.
- Camilo, F., Thorsett, S. & Kulkarni, S.R. 1994, *ApJL*, 421L, 15.
- Camilo, F., Nice, D. J. & Taylor, J.H. 1996, *ApJ*, 461, 812
- Chernoff, D. F. & Cordes, J. M. 1996a, in preparation.
- Chernoff, D. F. & Cordes, J. M. 1996b, in preparation.
- Cook, G. B., Shapiro, S. S. & Teukolsky, S. A. 1994a, *ApJ*, 423, L117.
- Cook, G. B., Shapiro, S. S. & Teukolsky, S. A. 1994b, *ApJ*, 424, 823.
- Cordes, J. M. 1986, *ApJ*, 311, 183.
- Cordes, J. M., Weisberg, J. M. & Boriakoff, V. 1985, *ApJ*, 288, 221.
- Cordes, J. M., Wolszczan, A., Dewey, R.J., Blaskiewicz, M. & Stinebring, D. R., 1990, *ApJ*, 349, 245.
- Cordes, J. M. & Lazio, T. J. W. 1991, *ApJ*, 376, 123.
- Cordes, J. M., Weisberg, J. M., Frail, D. A., Spangler, S. R. & Ryan, M. 1991, *Nature*, 354, 121.
- Cordes, J. M. & Chernoff, D. F. 1996, in preparation.
- Dewey, R. J., Cordes, J. M. & Wolszczan, A. 1988, in *Radio Wave Scattering in the Interstellar Medium*, eds. J. M. Cordes, B. J. Rickett & D. C. Backer, AIP, p. 217.
- Foster, R. S. & Tavani, M. 1992 in *X-ray Binaries & Recycled Pulsars*, NATO ASI, (Dordrecht: Kluwer), eds. E. P. J. van den Heuvel & S. A. Rappaport, 377, p. 437.

- Foster, R. S., Cadwell, B.J., Wolszczan, A. and Anderson, S. B. 1995, ApJ, 454 , 826
- Frail, D. & Weisberg, J. M. 1990, AJ, 100, 743.
- Fruchter, A. S. & Goss, W. M. 1990, ApJ, 365, L63.
- Harding, A.K. 1984, in Millisecond Pulsars, Proceedings of NRAO Worshop, (NRAO), eds. S. P. Reynolds & D. R. Stinebring, p. 113.
- Haslam, C.T.G., Salter, C.J., Stoffel, H. & Wilson, W.E. 1982, A&ASuppl, 47, 1.
- Johnston, H. M. & Kulkarni, S. R. 1991, ApJ, 368, 504.
- Johnston, H. M., Kulkarni, S. R. & Phinney, E. S. 1992, in *X-ray Binaries & Recycled Pulsars*, NATO ASI, (Dordrecht: Kluwer), eds. E. P. J. van den Heuvel & S. A. Rappaport, 377, p. 349.
- Kaspi, V.M. & Stinebring, D.R. 1992, ApJ, 392, 530.
- Kaspi, V.M., Taylor, J.H. & Ryba, M. 1994, ApJ, 428, 713.
- Kulkarni, S.R. & Narayan, R. 1988, ApJ, 335, 755.
- Loredo, T. J. & Wasserman, I. 1995, ApJSupplement, 96, 261.
- Lorimer, D. R., Bailes, M., Dewey, R. J. & Harrison, P. A. 1993, MNRAS, 263, 403.
- Lorimer, D. R. *et al.* , 1995, ApJ, 439, 933.
- Lorimer, D. R. 1995, MNRAS, 274, 300.
- Lundgren, S.C., Zepka, A. & Cordes, J.M. 1995, ApJ, 453 , 419.
- Lyne, A.G. & Lorimer, D. R. 1994, Nature, 369, 127.
- Lyne, A.G. & Manchester, R. N. 1988, MNRAS, 234, 477.
- Lyne, A.G., Manchester, R. N. & Taylor, J.H. 1985, MNRAS, 213, 613.
- Manchester, R. N. 1994, in *Millisecond Pulsars: A Decade of Surprise*, Eds. A.S. Fruchter, M. Tavani & D.C. Backer., ASP Conference Series, 72, 3.
- Narayan, R. 1987, ApJ, 319, 162.
- Naylor, T. & Podsiadlowski, Ph. 1993, MNRAS, 262, 929.
- Navarro, J., de Bruyn, A.G., Frail, D.A., Kulkarni, S.R. & Lyne, A.G. 1995, ApJ, 455, 55.
- Nicastro, L. & Johnston, S. 1995, MNRAS, 273, 122.
- Nicastro, L., Lyne, A.G., Lorimer, D. R., Harrison, P.A., Bailes, M. & Skidmore, B. D. 1995, MNRAS, 273, L68.
- Nice, D. J. & Taylor, J.H. 1995, ApJ, 441, 429.
- Nice, D. J., Fruchter, A.S. & Taylor, J.H. 1995, ApJ, 449, 156.
- Paczynski, B. 1990 ApJ, 348, 485.
- Phinney, E.S. & Kulkarni, S.R. 1994, ARA&A, 32, 591.
- Phinney, E.S. & Blandford, R. D. 1981, MNRAS, 194, 137.

- Rankin, J.M. 1983, ApJ, 274, 333.
- Rankin, J.M. 1993, ApJ, 405, 285.
- Rickett, B. J. 1990, ARA&A, 28, 561.
- Ruderman, M.A. & Shaham, J. 1983, *Comments on Modern Physics*, Part C, 10, 15.
- Stinebring, D.R. & Condon, J.J. 1990, ApJ, 352, 207.
- Taylor, J. H. & Weisberg, J. M. 1989, ApJ, 345, 434.
- Taylor, J. H. & Cordes, J. M. 1993, ApJ, 411, 674.
- Taylor, J. H., Manchester, R. M., & Lyne, A. G. 1993, ApJS, 88, 529.
- Thomas, P. 1989, MNRAS, 238, 1319.
- Thorsett, S.E., Deich, W.T.S., Kulkarni, S.R., Navarro, J., and Vasisht, G. 1993, ApJ, 416, 182.
- van Paradijs, J. & White, N. 1995, ApJL, 447, L33.
- Vivekenand, M. & Narayan, R. 1981, J. Ap. Ast., 2, 315.
- Webbink, R.F. and Kalogera, V. 1994, “The Origin of Low Mass X-Ray Binaries”, in *The Evolution of X-Ray Binaries*, AIP Conf. 308, eds. S. S. Holt and C. S. Day, 321.
- Wielen, R. 1977, A&A, 263, 275.
- Wijers, R. A. M. J. & van Paradijs, J. 1991, A&A, 241, L37.
- Wolszczan, A. 1990, IAU Circ. 5073
- Wolszczan, A. 1991, Nature, 350, 688.
- Wolszczan, A. 1994, Science, 264, 538.

Table 1:

MSP Survey Parameters

Survey (1)	Site (2)	ν (GHz) (3)	Ω_S (deg 2) (4)	N_{MSP} (5)	S_{sys} (Jy) (6)	S_{min_0} (mJy) (7)	Ref (8)
1	A	0.43	680	3	3	0.5	1
2	A	0.43	235	4	3	1.0	2
3	A	0.43	250	0	3	0.4	3
4	A	0.43	7	1	3	0.2	4
5	A	0.43	682	2	3	0.7	5
6	A	0.43	150	1	3	0.4	6
7	P	0.44	20,600	10	90	3.0	7
8	J	0.41	1,650	1	70	3.1	8

Sites: A = Arecibo, J = Jodrell Bank, P = Parkes.

References: (1) Camilo et al. 1996; (2) Nice et al. 1995; (3) Thorsett et al. 1993; (4) Lundgren et al. 1995; (5) Foster et al. 1995; (6) Wolszczan 1990; (7) Manchester et al. 1996; (8) Nicastro et al. 1995.

Table 2:

Millisecond Pulsars Used

MSP Name	ℓ (deg)	b (deg)	P (ms)	$\log \Delta P$ (ms)	S (mJy)	ΔS (mJy)	D_L (kpc)	D_U (kpc)	Ref
(1)	(2)	(3)	(4)	(5)	(6)	(7)	(8)	(9)	(10)
J0034–0534	111.5	−68.1	1.88	−10.7	16	5	0.74	1.23	7
J0437–4715	253.4	−42.0	5.76	−11.4	600	180	0.105	0.175	7
J0613–0200	210.4	−9.3	2.19	−11.4	21	6	1.64	2.74	7
J0711–6830	279.5	−23.4	5.49	−4.1	7	2	0.77	1.29	7
J0751+1807	202.7	21.1	3.48	−11.0	10	3	1.51	2.53	4
J1012+5307	160.3	50.9	5.26	−10.7	30	9	0.39	0.65	8
J1045–4509	280.9	12.3	7.47	−10.7	20	6	2.43	4.05	7
B1257+12	311.3	75.4	6.22	−12.7	20	6	0.47	0.77	6
J1455–3330	330.7	22.6	7.99	−10.2	13	4	0.56	0.93	7
J1640+2224	41.1	38.3	3.15	−12.3	12	4	0.88	1.48	5
J1643–1224	5.7	21.2	4.62	−10.5	75	23	4.84	∞	7
J1713+0747	28.8	25.2	4.57	−12.1	36	10	0.8	1.6	5
J1730–2304	3.1	6.0	8.12	−10.5	43	13	0.38	0.64	7
B1855+09	42.3	3.1	5.36	−12.5	31	9	0.70	1.30	2
B1937+21	57.5	−0.3	1.56	−12.7	240	72	3.60	15.7	2
B1957+20	59.2	−4.7	1.61	−12.52	20	6	1.15	1.91	2
J2019+2425	64.7	−6.6	3.93	−12.7	15	5.0	0.68	1.14	2
J2124–3358	10.9	−45.4	4.93	−10.2	20	6	0.18	0.30	7
J2145–0750	47.8	−42.1	16.05	−9.7	50	15	0.38	0.62	7
J2317+1439	91.4	−42.4	3.45	−12.7	14	5	1.4	2.3	1
J2322+2057	96.5	−37.3	4.81	−12.6	4	2	0.5	1.1	1
J2229+2643	87.7	−26.3	2.98	−12.1	18	5	1.0	2.0	1

References: (1) Camilo et al. 1996; (2) Nice et al. 1995; (3) Foster et al. 1995; (4) Lundgren et al. 1995; (5) Thorsett et al. 1993; (6) Wolszczan 1990; (7) Manchester et al. 1996; (8) Nicastro et al. 1995.

Table 3:

Best-fit Disk Models

Parameter	Gaussian in z	Exponential in z	Gaussian in V	units
α_P	2.0 ± 0.33	2.0 ± 0.33	2.0 ± 0.33	—
α_{L_p}	2.0 ± 0.2	2.0 ± 0.2	2.1 ± 0.2	—
σ_z	$0.65^{+0.16}_{-0.12}$	$0.50^{+0.19}_{-0.13}$	—	kpc
$\sigma_{z,birth}^\dagger$	—	—	0.1	kpc
σ_V	—	—	52^{+17}_{-11}	km s ⁻¹
n_d	29^{+17}_{-11}	44^{+25}_{-16}	53^{+28}_{-18}	kpc ⁻³
N_d	52^{+29}_{-19}	49^{+27}_{-18}	49^{+27}_{-17}	kpc ⁻²
P_1	> 1.0 (95%) > 0.65 (99%)	> 1.0 (95%) > 0.65 (99%)	> 1.0 (95%) > 0.70 (99%)	ms
L_{p1}	$1.1^{+0.4}_{-0.5}$	$1.1^{+0.4}_{-0.5}$	$1.1^{+0.4}_{-0.5}$	mJy kpc ²

Confidence intervals, except where noted, are two-sided 68% intervals. \dagger fixed parameter.

Table 4:

Disk + Diffuse Models

Model	Diffuse only		Disk + Diffuse		
	\hat{n}_h (kpc $^{-3}$)	$\frac{\mathcal{L}(0, \hat{n}_h)}{\mathcal{L}(\hat{n}_d, 0)}$	\hat{n}_d (kpc $^{-3}$)	\hat{n}_h (kpc $^{-3}$)	$\hat{n}_h(R_0)$ (kpc $^{-3}$)
uniform density	1.5	$10^{-21.3}$	38	< 0.42 (90%) < 0.84 (99%)	..
$r_h = 1$ kpc $s_h = 7/2$	4080	$10^{-16.4}$	38	< 1520 (90%) < 3040 (99%)	< 0.83 < 1.66
$r_h = 5$ kpc $s_h = 2$	10.8	$10^{-15.1}$	38	< 3.3 (90%) < 6.7 (99%)	< 0.31 < 0.62

Table 5:

Velocity Moments for Nearby Pulsars

	σ_V (km s ⁻¹)	σ_z (kpc)	\bar{v}_R	$\bar{\delta v}_R$	\bar{v}_t	$\bar{\delta v}_t$	\bar{v}_z	$\bar{\delta v}_z$
Uniform Surface Density (independent of R):								
20	0.05	0.02	1.28	0.00	0.86	-0.00	0.70	
	0.15	0.01	1.28	-0.00	0.86	-0.00	0.79	
40	0.05	0.00	1.26	-0.11	0.80	-0.00	0.66	
	0.15	0.01	1.26	-0.11	0.80	-0.01	0.69	
60	0.05	0.00	1.18	-0.22	0.77	0.00	0.64	
	0.15	0.00	1.18	-0.22	0.77	-0.00	0.65	
80	0.05	0.01	1.09	-0.29	0.75	0.00	0.61	
	0.15	0.00	1.09	-0.30	0.75	0.00	0.61	
100	0.05	0.01	1.01	-0.35	0.74	0.00	0.58	
	0.15	0.00	1.00	-0.35	0.74	0.00	0.58	
Exponential Surface Density (in R):								
20	0.05	0.03	1.24	-0.17	0.83	-0.01	0.69	
	0.15	0.01	1.23	-0.17	0.83	-0.01	0.79	
40	0.05	-0.01	1.17	-0.31	0.78	-0.00	0.63	
	0.15	0.01	1.17	-0.31	0.78	-0.00	0.66	
60	0.05	-0.01	1.09	-0.41	0.73	-0.00	0.58	
	0.15	0.00	1.09	-0.41	0.74	0.00	0.60	
80	0.05	0.00	1.03	-0.47	0.69	-0.00	0.55	
	0.15	0.01	1.02	-0.47	0.70	0.00	0.56	
100	0.05	0.01	0.97	-0.50	0.66	-0.00	0.51	
	0.15	0.00	0.96	-0.50	0.66	0.00	0.52	

Velocity moments for particles of Galactocentric radius $7.5 < R < 9.5$ kpc and $|z| < 3$ kpc. Here \bar{v}_R means $\langle v_R \rangle / \sigma_V$, $\bar{\delta v}_R$ means $\sqrt{\langle (v_R - \langle v_R \rangle)^2 \rangle} / \sigma_V$, and so on. The top section refers to a disk with constant birth density in R ; the bottom section to a disk with birth density varying with exponential scale length 3.5 kpc in R . All moments given in units of σ_V . Numerical accuracy of ± 0.02 for all entries. All mixed second order moments are zero to ± 0.03 .